# Utilising publicly available datasets for identifying offshore salt strata and developing salt caverns for hydrogen storage

Accepted Manuscript

*Geological Society, London, Special Publications*

# Utilising publicly available datasets for identifying offshore salt strata and developing salt caverns for hydrogen storage

Craig Allsop, Georgios Yfantis, Evan Passaris & Katriona Edlmann

DOI: https://doi.org/10.1144/SP528-2022-82

To access the most recent version of this article, please click the DOI URL in the line above. When citing this article please include the above DOI.

Received 12 March 2022
Revised 7 November 2022
Accepted 8 November 2022



Supplementary material at https://doi.org/10.6084/m9.figshare.c.6315742

**Correction notice:** this correct version of the Accepted Manuscript replaces a previous version uploaded in error

# Utilising publicly available datasets for identifying offshore salt strata and developing salt caverns for hydrogen storage

**Craig Allsop[1], Georgios Yfantis[2], Evan Passaris[2] and Katriona Edlmann[1]**

[1]School of Geosciences, The University of Edinburgh, UK

[2]SNC-Lavalin's Atkins business

*Highlights:*

- Solution-mined salt caverns can provide additional offshore energy storage capacity for the UK.
- Methodology established for offshore salt cavern site selection process, implementing a robust and forensic geological screening.
- Improved hydrogen storage capacity estimates for bedded and diapiric salt domains in the Southern North Sea.
- Storage potential is thermodynamically derived, with respect to geomechanical and geospatial exclusions.
- Potential hydrogen storage capacity of 292 $TWh_{H2}$ in offshore Southern North Sea salt caverns.

Key Words: energy storage, offshore salt caverns, hydrogen, Net Zero

**Abstract**

Hydrogen is expected to play a key role in a future climate-neutral economy by decarbonising 'hard to abate' sectors, and importantly act as an energy carrier to balance intermittent renewable energy production which if stored, could be used to address grid-scale energy demands. It is evident that for unlocking the vast potential of hydrogen technologies, large-scale hydrogen storage with the capability of fast cyclic operations needs to be secured.

Underground salt caverns, where decades of operational experience exist, offer an attractive option for hydrogen storage due to the; high hydrogen sealing potential of salt, capability for large injection/withdrawal flow rates and capacity for large volume storage.

This study presents a novel methodology for selecting offshore salt cavern sites based on publicly available datasets, which leads to eventually estimating regional hydrogen storage capacities. The Southern North Sea was investigated and a case study detailing a single diapiric salt structure is presented, demonstrating the strength and practicality of the framework as well as highlighting the potential of offshore salt cavern storage of hydrogen in the decarbonisation energy journey of the UK.

## 1. *Introduction:*

The recent UK Hydrogen Strategy recognises the 'critical' role of hydrogen for achieving Net Zero and meeting up to a third of the UK's energy demand by 2050 (HM Government, 2021). It is included in all climate-neutrality scenarios within the UK's ambitious decarbonisation timeline ('Net Zero by 2050'), with hydrogen identified as being particularly well suited to decarbonising: 'hard to abate' heavy industry, sectors of long-distance transportation i.e., heavy-duty vehicles, railways, and shipping, and heating gas grid, with the end goal being addressing the energy trilemma, 'security, affordability, and sustainability' (Committee on Climate Change, 2020).

Hydrogen is an energy carrier that can be produced via electrolysis utilising renewable energy sources, i.e., wind turbines (Li *et al.,* 2018). Steam-methane reforming (SMR) is another leading technology for the production of industrial scale quantities of Hydrogen (Bartholomew & Farrauto, 2006 and Caglayan *et al.,* 2020), however without carbon capture and storage it is not considered low carbon. Large scale hydrogen storage, can ensure that renewable energy sources will be utilised to their full capacity, balancing the mismatch between energy supply and demand. Stored hydrogen can be used to address the daily and seasonal peaks and troughs of the energy demand curve. There are many hydrogen storage technologies, and each has a role to play within the energy system. Accounting for the storage volume and discharge capacity these technologies have to offer, it may be concluded that the envisioned long term inter-seasonal storage with GW to TW output and discharge over weeks to months, can only be delivered by geological storage in underground salt caverns, depleted gas fields and deep saline aquifers (Hassanpouryouzband, *et al.* 2021). In that realm, the UK Continental Shelf (UKCS) will be crucial in providing these large-scale geological energy storage facilities.

Underground salt cavern storage has been identified as one of the most promising geological storage technologies to pioneer the initial integration of hydrogen into the UK's energy mix (Energy Technologies Institute, 2015), thus enabling the kickstart and growth of the anticipated hydrogen economy. The physical properties and operational potential of rocksalt provides salt caverns with:

- a high hydrogen sealing capability;
- an inert chemical behaviour with respect to hydrogen;
- relatively homogeneous and isotropic properties; and
- an ability to endure cyclic loading storage operations.

Around the globe salt caverns store a wide range of gases and liquids that are utilised either as feedstock or for seasonal trading and strategic energy reserves (Williams *et al.,* 2022). Hydrogen storage in salt caverns has been successfully implemented in Teesside, UK since the 1970's (Evans *et al.,* 2021 and Williams *et al.,* 2022) with further examples existing in the Moss Bluff and Clements domes, USA, demonstrating the feasibility and resilience of the technology (Landinger & Crotogino, 2007; Panfilov, 2015; Czapowski and Tarkowski, 2018; Hévin, 2019 and Portarapillo & Di Benedetto, 2021).

Salt caverns are developed through solution mining underground salt deposits and can achieve volumes of 1,000,000 $m^3$ (Plaat, 2009 and Bünger *et al.,* 2016). This, in combination with their maximum operating pressure reaching values corresponding to 80% of the geostatic pressure (Ozarslan, 2012 and Stolzenburg *et al.*, 2014), allows for storage of large hydrogen volumes (e.g.,

>200 $GWh_H$). Achieving the envisioned storage volumes and overcoming onshore geographical limitations, environmental impacts caused by surface tanks as well as public concerns (Caglayan *et al.*, 2020; Evans *et al*., 2021; Lankof *et al.,* 2022 and Valle-Falcones *et al.,* 2022) could be accomplished by developing salt caverns offshore.

Currently, no offshore salt cavern gas storage facility exists in the extensive salt deposits of the Zechstein Supergroup which is prominent throughout the entire Permian Basin of Northern Europe (Maystrenko *et al.*, 2012, 2013 and Grant *et al.*, 2019). Specifically, in the vicinity of the UK, extensive Zechstein halite beds are present offshore along the eastern and northern coastlines (Evans & Holloway, 2009; Parkes *et al.,* 2018; Grant *et al.*, 2019 and Williams *et al.,* 2022). Furthermore, while there are published assessments of onshore Zechstein deposits for energy storage in salt caverns (Beutel & Black, 2005; Evans & Holloway, 2009; Howard *et al.*, 2009; Parkes *et al.*, 2018 and Williams *et al.,* 2022), there is a significant lack of assessment of Southern North Sea offshore Zechstein site and cavern selection assessments for energy storage. Williams *et al.* (2022) highlight the additional large storage volume potential the UKCS salt deposits possess as future offshore hydrogen storage alternatives and their importance. Furthermore, a report produced by the BGS identified salt thicknesses and characterised suitable Zechstein formations as gas storage facilities, however, the identified salt volumes suitable for salt cavern development were generally deemed too deeply buried (Smith *et al.,* 2005).

The Gateway project in the East Irish Sea is the only known offshore salt cavern energy storage project that was planned in the UK which, however, did not mature for commercial reasons. Its target salt was the Triassic Preesall Halite which is known to have limited salt volumes when compared to the Southern North Sea salt basin (Parkes *et al.*, 2018). However, offshore salt caverns, with wellheads positioned onshore will be established with directional drilling and are set to be developed at Larne Lough, Northern Ireland (Passaris & Wood, 2019). Tractebel and partner companies have recently delivered a media release stating the development of the world's first offshore hydrogen storage concept in offshore salt caverns, highlighting the reality and feasibility of this storage technology opportunity (Tractebel, 2021). Furthermore, dCarbonX and ESB have made a joint announcement of their partnership to develop a green hydrogen storage project centred around the Poolbeg peninsula in Dublin (ESB, 2021).

The UKCS has the potential to develop a strong integration of synergies through the coupling of hydrogen salt cavern storage, large-scale wind farms and floating electrolyser facilities, in addition to integrating into the gas production, reforming (SMR) and geological storage of carbon dioxide industry (Williams *et al.,* 2022). Offshore salt cavern hydrogen storage is a technology that can link these currently ‘isolated’ low carbon technologies into one single, highly efficient energy and carbon mitigating system.

This paper presents a novel methodology for offshore salt cavern site selection and cavern development, utilising a diverse suite of publicly available offshore licence datasets and analytical techniques. It forms a practical foundation implementing a stepwise approach, the capability of which is demonstrated by presenting a case study that focuses on the Audrey Salt Wall in the Southern North Sea (SNS) Zechstein Supergroup salt formations (Realey *et al.,* 2003 and Elam, 2007). The study discusses internal geometries and geological heterogeneities, as well as the development of caverns in terms of geomechanical requirements and the resulting storage capacity estimates, while demonstrating the level of reliance of results.

This study focuses on the SNS, which is an ideal area to demonstrate and evaluate the offshore salt cavern site selection and hydrogen storage capacity methodology. This is due to its extensive salt deposits, availability of a large subsurface exploration database, juxtaposition with existing oil and gas infrastructure and proximity to the Teesside industrial clusters. In addition, there are a growing number of offshore wind farm projects in the SNS (e.g., the 1,218 MW Hornsea One) that highlight the potential of the Zechstein Supergroup to facilitate *in situ* hydrogen storage alternatives. This prospect may be further supported if existing hydrocarbon infrastructure (e.g., platforms, pipeline, cable routes) can be repurposed, reducing the cost of decommissioning the hydrocarbon industry, in addition to lowering development costs of prospective engineered solution-mined salt cavern projects (Evans *et al.*, 2021).

## 2. *SNS evaporite deposits:*

The SNS is situated on the western side of the Southern Permian Basin (Tucker, 1991, and references therein). This region is characterised by thick deposits of rocksalt halite (NaCl) laid down around 250 million years ago during the Lopingian Epoch in the shallow and isolated Zechstein intercontinental basin that developed as the supercontinent of Pangaea began to rift apart (Grant *et al.*, 2019). The basin began a phase of steady subsidence followed by multiple cycles of catastrophic flooding and evaporation to form kilometre thick salt deposits which have experienced several phases of tectonism, resulting in extensive halokinesis of the Zechstein Supergroup (Smith, 1979; Warren, 2006 and Grant *et al.*, 2019).

The Zechstein Supergroup is composed of five cycles (Z1-Z5), consisting of four main carbonate-evaporite sequences and a fifth rudimentary cycle (Tucker, 1991 and Grant *et al.*, 2019). The second and succeeding cycles are dominated by evaporites that display an upward transition from anhydrite ($CaSO_4$) to halite and then magnesium or potassium salts (K-Mg salts) (Fig. 1) (Tucker, 1991 and Smith *et al.*, 2005). The cycles become increasingly more saline in response to repeated, cyclic evaporation and recharge of the saline basin (Geluk, 2005; Peryt *et al.*, 2010 and Grant *et al.*, 2019). Each cycle displays lateral facies variations from the basin margins to centre; carbonate-rich and anhydrite formations were deposited at the margins and on intra-basin structural highs during highstands, while thick halite-rich and K-Mg-rich evaporites deposited in the deeper basins, during lowstands (Tucker, 1991).

The SNS is vertically dominated by three rocksalt formations; the Stassfurt Halite Formation (Z2), Leine Halite Formation (Z3), and the Aller Halite Formation (Z4), which themselves can be divided into multiple subgroups (Tucker, 1991 and Cameron *et al.*, 1992). The Z2, Z3 and Z4 halite formations are identified as the most suitable for hydrogen salt cavern storage as they comprise suitable thicknesses of relatively homogeneous halite and K-Mg salts (Fig. 1). They tend to have very few insolubles, and only occasionally segmented by a series of anhydrite, carbonate, and mudstone formations (Tucker, 1991; Warren, 2006; Van Gent *et al.*, 2011; Strozyk *et al.*, 2014 and Zijp *et al.*, 2018).

The SNS is the largest salt basin situated in the UK and is characterised by major salt halokinetic deformation. Several phases of post-Permian tectonism have resulted in extensive Zechstein salt mobilisation and the creation of salt walls and diapirs reaching several kilometres in thickness towards the basin centre (Maystrenko *et al.*, 2012, 2013 and Strozyk *et al.*, 2014). These diapiric structures form due to the chemo-physical properties of salt when it is buried, where its bulk density

remains around 2.2 g/cm$^3$, whereas the density of the surrounding sediments increases with depth (Gevantman, 1981). At depths below 1,000 m salt tends to be less dense than its overburden and can diapirically rise due to buoyancy if stress conditions create an imbalance in the overburden. These imbalances are initiated by differences in elevation at the salt/overburden interface, differential loading (effectively a hydraulic head) and tectonic stresses (Glennie, 1990 and Warsitzka *et al.*, 2015). In the SNS, early-stage structural evolution of the Zechstein Supergroup was dominated by major phase tectonic extension during the Early Triassic creating NW-SE trending salt ridges. These structures were later reorganised due to regional shortening in the Late Cretaceous, which led to the lateral and vertical transfer of large salt volumes, generating tall salt diapirs (Harding & Huuse, 2014 and Adam *et al.,* 2017). Heterogeneous distribution of these imbalances across the SNS has consequently resulted in regions characterised by low salt mobilisation, where the Zechstein deposits are dominated by massively bedded halite deposits and salt pillows (Figs. 1 and 10), and regions that have undergone extensive halokinesis dominated by highly deformed, large salt domes, walls, and diapirs (Figs. 2, 10 and 11). There is a difference in salt mobility between different Zechstein evaporites, for example anhydrite is considered relatively immobile and deforms in a brittle manner in comparison with halite (Van Gent *et al.,* 2011 and Zijp *et al.*, 2018). Within the Zechstein halite deposits differences in mobility are observed which are a result of internal heterogeneities such as water content, differences in the crystal lattice and impurities (salt chemistry), with the Z2 (Stassfurt) halite regarded as the most mobile Zechstein salt unit within the SNS (Urai *et al.*, 2008; Jackson *et al.*, 2015; Jackson & Hudec, 2017 and Zijp *et al.*, 2018). Due to the lower stratigraphic positioning of the Z2 salt its migration drives mobility within the entire Zechstein Supergroup (Zijp *et al.*, 2018). Therefore, the less dense, purer and older, buoyant horizons migrate to the top and form the core of many diapiric structures (Fig. 2) (Ter Heege *et al.*, 2005a & 2005b; Urai *et al.*, 2008; Jackson *et al.*, 2015 and Zijp *et al.*, 2018). This buoyancy driven internal organisation of salts within diapir structures is supported by detailed interpretation of analogous diapiric salt structures such as the Gorleben and Góra salt diapirs in Northern Europe, which appear to have a chaotic internal structure, however, when investigated closer, the Zechstein cycles have a near ordered positioning with respect to one another (Von Berlepsch, 2017 and Cyran, 2020). Thus, high salt mobilisation can result in the creation of more favourable and suitable salt configurations of thick homogeneous halite located at desirable depths for salt cavern engineering. Supporting this statement, is a general rule of thumb that for diapirs forming an anticlinal geometry, the lowermost salt layers (i.e., Z2 salts) rise upwards in the core of the diapir, pushing outwards the overlying salt layers (Richter-Bernburg, 1980; Jackson *et al.,* 1990; Chemia *et al.,* 2009; Burliga, 2014; Strozyk *et al.,* 2014; Jackson *et al.,* 2015 and Pichat, 2022). This deformation characteristic is commonly observed in mined German and Polish Zechstein diapirs, where the Z2 salts form the core of the diapir and are surrounded by Z3 and Z4 salts that are restrained to the outer limit of the diapir (Fig. 2) (Burliga, 2014; Czapowski and Tarkowski, 2018 and Pichat, 2022). It is worth noting that the Z3 & Z4 halites are still suitable for cavern development and in many locations are indistinguishable from the Z2 cycles and should therefore still be considered for salt cavern engineering. Where diapiric systems that do not have lower Z2 salt formations in their core, first order folding patterns (as shown in Figure 2) may not exist. Instead, more complex internal folding, deformation patterns and intra-salt heterogeneities exist (Pichat, 2022 and Duffy *et al.,* 2022). In this case, a greater number of exploration wells are required to determine the location for salt cavern development. Ultimately, due to the nature of salt tectonic processes each salt basin and their respective diapirs will develop unique deformation patterns. Therefore, further offshore ground investigations are always required

to successfully deploy salt caverns as an alternative storage technology. However, as a preliminary and first order investigation, existing knowledge of internal salt structures from onshore European salt diapirs can be used to identify the localities suitable for further ground investigations and cavern development. At the edge of the basin, minor salt mobilisation has occurred and bedded salt structures resembling the original depositional stratigraphy are present. Smaller, suitable salt volumes are present; however, these regions are subject to heterogeneous lateral and vertical formation thicknesses (Figs. 1 and 10).

3. *Methodology & SNS basin evaluation:*

This section introduces the data and highlights the qualitative and quantitative suite of techniques that were used to develop a new methodology for both offshore salt cavern site selection and hydrogen storage capacity estimates (refer to Fig. 3). These methods utilised a diverse and well-established range of publicly available datasets from sources including the British Geological Survey (BGS), the North Sea Transition Authority National Data Repository (NSTA NDR), and peer reviewed scientific research papers. The use of multiple high-quality datasets enabled cross comparison between different data sources ensuring a high degree of confidence in the underlying data quality. This has encouraged the identification of potential limitations, allowing for a robust and high quality forensic geological investigations into the Zechstein salt formations to be undertaken (Figs. 3 and 9). The potential of offshore salt cavern hydrogen storage facilities was then confidently estimated as a first order investigation. The site selection and hydrogen storage capacity estimate methodologies developed during this study are applicable to any geographical region with evaporite deposits. For this paper, we assessed the UKCS Zechstein deposits to determine the hydrogen storage potential in offshore salt caverns within the UK SNS basin with a more detailed investigation undertaken on a single diaper (The Audrey Salt Wall).

Fig. 3 summarises the offshore salt cavern site selection process beginning with characterising the salt deposits, then moving onto constraining the limits of salt deemed suitable for cavern development through proximity analysis of existing infrastructure and finally onto cavern design, placement and storage capacity estimates. This figure highlights that determining the potential for salt cavern development requires:

- the utilisation of multiple techniques and datasets to form a robust analysis of the geology and geophysics of salt formations,
- the geomechanics associated to ensure cavern stability and,
- subsequent energy security.

Therefore, the characterisation of identified salt formations and their evaluation concerning their suitability for hydrogen storage are the first steps in the screening process.

The selection process for cavern emplacement depth and height was based upon the lithological heterogeneity, formation thickness and salt domain: bedded or structural (e.g., pillows, domes, and walls) (Fig. 10). This was determined from structural and stratigraphic assessment of seismic and well data from the SNS. Furthermore, cavern placement was based upon an optimal depth range, dependent on cavern convergence rate, hydrogen storage pressure, thickness of the hanging and foot-wall and recommended cavern shape criteria established from past literature and underground gas storage experience (Fig. 5 and Table 2). Using the recommended spatial parameters stated in Table 2, a distribution analysis using a gridding technique that **Parkes** *et al.* (2018) applied derived a

first estimate of the total number of caverns possible within a defined region after cavern design selection. This number was later refined using the process stated in Section *Regional storage volume corrections*. Finally, cavern capacity estimations of the storage potential were thermodynamically derived, defined by non-transient cavern temperature but fluctuating cavern pressure over time. Due to offshore storage options being the focus of this study, a land eligibility assessment was not carried out, instead the proximity of the chosen site to existing infrastructure was considered, with the aim to reduce the economical capital of future projects.

### 3.1. *Datasets utilised:*

Geo-referenced and digitised geological maps of the entire Permian Basin, specifically the Zechstein Supergroup (4 km distance between grid nodes), by Maystrenko *et al*. (2012 and 2013), allowed a first identification of locations where underground salt cavern development could be possible. Borehole log data and peer reviewed published geological map information from the Petroleum Geo-Services (PGS) North Sea Digital Atlas, created by the BGS, permitted verification of the top, base, and isopach maps of the Zechstein Supergroup, ensuring that the highest quality dataset and geological maps formed the basis of this study.

The rich legacy of seismic and well data from the NSTA NDR was used to correlate existing Zechstein Supergroup maps, further refining the locations best suited for salt cavern development. To undertake the SNS case study for testing the methodology developed in this work, 3D seismic data from the 'PGS SNS MegaSurvey Version 2.0 (2016)' was primarily utilised to investigate internal salt geometries and intra-salt heterogeneities of the Zechstein Supergroup. The seismic data is a large-scale, merged post-stack 3D dataset consisting of public and PGS-owned 3D data rebinned to a common grid (UTM 31N) and matched to produce a phase-balanced and uniformly scaled contiguous regional 3D dataset of the SNS gas basin (Petroleum Geo-Services Reservoir, 2016). Information on the seismic data input, resolution and processing can be found within the 'Final SNS MegaSurvey Processing Report' (Petroleum Geo-Services Reservoir, 2016). In regions of high salt mobilisation, steeply dipping complexly shaped salt structures lead to limitations to the resolution of the seismic data within the Zechstein Supergroup salt formations. Limitations include reduced frequency content as depth increases, seismic opaqueness and featureless, or incoherent/chaotic seismic facies that lack internal reflectivity. These resolution limitations have a significant impact in determining the salt edges. Borehole log data was used to determine changes in Zechstein Supergroup composition and localities (e.g., depth, location within salt structure) most suitable for the development of a salt cavern.

### 3.2. *Subsurface salt visualisation:*

The geology at the edge of salt structures is commonly disturbed and of poor geomechanical quality making its identification crucial for positioning caverns (Evans, 2007). Due to these disturbed zones having the capability to penetrate several hundred feet into the salt body, a buffer distance of 500 m was implemented from the edge of each diapiric salt deposit to ensure salt cavern development in theoretically favoured conditions (Kupfer *et al.*, 1998 and Caglayan *et al.,* 2020). The discussed resolution limitations also add to the difficulty of distinguishing the various Zechstein Supergroup formations. To address them the seismic data was compared to regional well data. Time-depth calibration was determined from the analysis of time-depth relationships from available well database checkshot surveys (Supp. 1).

Initial characterisation of well data utilised lithological, mud, composite, gamma ray (GR), and density logs to characterise the internal make-up, highlighting the lithological heterogeneities of the Zechstein Supergroup (Fig. 8), in addition to differentiating between bedded and diapiric salt domains. This allowed for the identification of stringers composed of layers or fragments of rock comprising minerals other than halite (e.g., anhydrite, carbonates and/or mudstones) (Figs. 2 and 8), associated with particular Zechstein formations (e.g., the Z3 cycle contains a distinctive relatively brittle layer of anhydrite-carbonate) (Warren, 2006; Van Gent *et al.*, 2011; Strozyk *et al.*, 2014 and Zijp *et al.*, 2018).

To define the petrophysical differences between pure halite and common non-salt and K-Mg salt interbeds, GR logs were used to define these lithological differences. GR logs are commonly used for identifying shale content, measuring the concentration of radioactive elements in clay minerals (Parkes *et al.,* 2018). Halite dominantly consists of NaCl and contains little mudstone content and therefore has a very low GR reading and is easily distinguishable from any mudstone interbeds (Table 1) (Schlumberger, 1991; Urai *et al.,* 2008 and Parkes *et al.,* 2018). K-Mg salts have relatively high GR log values and therefore, other wireline logging tools such as density logs were used to define the differences in these lithologies (Table 1) (Schlumberger, 1991 and Parkes *et al.,* 2018).

Where boreholes penetrate large, highly deformed diapiric salt structures, differentiation between the individual Zechstein cycles was difficult, however, where possible interpretations were made. In many areas with poor seismic resolution, stringers were commonly the only markers identifiable, examples of which can be clearly observed on the Dutch continental shelf (Van Gent *et al.,* 2011).

The non-salt stringer and raft interlayers present in the lithological logs are highly unlikely to be continuous or extensive throughout the entire diapiric salt body and as such are unlikely to present a significant drilling and engineering challenge (Strozyk *et al.,* 2014). This is supported by the lack of any continuous seismic stringer or raft reflectors crosscutting the diapiric salt bodies, a minor degree of uncertainty remains in areas of poor seismic reflectivity (Van Gent *et al.,* 2011 and Strozyk *et al.,* 2014). In regions of low salt mobilisation (i.e., quadrant 41), the full stratigraphic sequence of the Zechstein Supergroup succession can be observed. These bedded salt formations typically display heterogeneous lateral variations (i.e., formation thickness variations) providing constrained opportunities for large volume (>500,000 $m^3$) salt cavern development.

It is important to note that the seismic and borehole data utilised was gathered for the purpose of hydrocarbon exploration, not salt cavern engineering. Therefore, although the data is of high quality, detailed cavern placement assessments require improvements in the pre-processing of the seismic data to minimise pitfalls and problems with seismic imaging (Jones & Davison, 2014). Importantly, evaluating the pre-processing parameters, pre-stack depth migration and integration with geological information is essential to improve imaging of salt complexes (Landrø *et al.*, 2001 and Davison *et al.,* 2013; Jones & Davison, 2014). However, poor image quality might not necessarily be related to velocity variation purely from compositional aspects. Non-reflective diapiric cores may represent salts of sylvite, carnallite and halite, which have been subject to intense isoclinal folding within the diapir neck, resulting in sub-vertical axes, reducing the reflectivity of the structure (Jones & Davison, 2014). Therefore, seismic opaqueness could be interpreted as a positive indicator for purer, more favourable salt compositions. Possible limitations related to borehole data from the hydrocarbon industry are discussed by Parkes *et al.* (2018).

Although there is a rich legacy of offshore licence datasets, when an offshore location is considered, data is generally only available from a small number of borehole penetrations, with a spacing

between boreholes of several kilometres. This, coupled with major salt mobility reduces the degree of certainty when tying borehole logs across diapiric salt structures tens of kilometres in length (Figs. 10 and 11).

### 3.3. *General cavern design demands:*

Once the optimal salt formation and suitable depth/thickness/infrastructure locality of the cavern is determined (refer to methodology shown in Fig. 3), a detailed analysis at the cavern scale is required to minimise uncertainties regarding cavern design, geomechanical stability and integrity of the cavern during hydrogen storage operation. The physical effects at the cavern wall are closely linked to the microscale responses of the host salt, which are a function of pressure, temperature, heterogeneity, and state of stress. The following cavern design is based upon extensive practical onshore cavern design experience (Fig. 4) (Crotogino *et al.*, 2001; Bérest & Brouard, 2003; Plaat, 2009; Evans & Holloway, 2009; Bérest, 2011; Ozarslan, 2012; Wang *et al.*, 2015b; Lux, 2009; Li *et al.*, 2020; Asgari *et al.*, 2020; Taheri *et al.*, 2020; Caglayan *et al.*, 2020 and Raith *et al.,* 2022). Key parameters have been determined for understanding the mechanical disturbances the cavern may be subject to, in addition to the principal stability parameters which maximise cavern stability and ensure the security and serviceability of the energy vector (i.e., hydrogen) (Table 2).

Additionally, the creep characteristics of rocksalt can have significant impact on the safety and stability of long-term operations of salt cavern underground gas storage. The convergence rate is dependent on temperature, rheological properties, neighbouring caverns, cavern design and the operational scenario of the cavern (Lankof *et al.,* 2022). For example, changes in storage capacity are to be expected, and the cavern response will be linked to the properties of the host salt formation and thermomechanical conditions during cavern operation (Wang *et al.,* 2015a; Ma *et al.,* 2021 and Lankof *et al.,* 2022). Lankof *et al.* (2022) estimate an average storage capacity loss of 33% in caverns located at the gas storage facility Mogilno, Poland over a 30-year period. Note that such estimations are case specific.

The halite deposits are evaluated over the depth ranges considered suitable for hydrogen storage operation, 500 m-2,000 m (Warren, 2006; Plaat, 2009; Evans & Holloway, 2009 and Caglayan *et al.*, 2020). This was based upon maximising the volume of hydrogen stored and the energy density capacity of the cavern with respect to salt creep rate and the associated rate of cavern convergence (Fig. 4 and Table 2). It has been suggested from work on onshore salt caverns (Poland), that to maximise hydrogen storage potential the optimum cavern centre depth was determined to be 1300 m below ground level (Lankof *et al.,* 2022).

The effects of cyclic loading on the elasticity and strength of geomaterials has long been studied (Haimson, 1974). Wang *et al.* (2021) determined that during energy storage operations in salt caverns, the elastic modulus increases then remains unchanged with the number of cycles. They also state that a threshold occurs, sample specific, for the number of cycles affecting the irreversible deformation during long-period cyclic loading.

The cyclic injection and withdrawal of compressed hydrogen causes fluctuations in the internal cavern pressure and temperature, which adversely affects the mechanical integrity and stability of the cavern. Geomechanical simulations conducted by Wassing *et al.* (2022) indicate that dilation and

tensile failure (spalling) of the cavern wall can occur during withdrawal periods whereby rapid decompression and cooling occurs. Furthermore, the violation of the effective tensile stress criterion is likely to increase during fast injection and withdrawal cycles (Minkley *et al.,* 2015). However, spalling has limited penetration into the cavern wall and is, therefore, unlikely to have significant impacts on long-term cavern integrity (Minkley *et al.,* 2015 and Wassing *et al.,* 2022). Finally, it must be noted that flow limits (different combinations of flow rates and durations against cavern pressure conditions) are implemented at cavern sites to avoid the development of tensile stresses (Passaris *et al.,* 2018)

The diffusion of hydrogen into the cavern wall may lead to alterations to the mechanical and creep properties of the rocksalt. Abuaisha and Billoiotte (2021) indicate that the loss of hydrogen via diffusion is very negligible, however, further experimental research is required to quantify and characterise these effects (Wassing *et al.,* 2022).

Recent geomechanical simulations of energy storage in salt formations investigate the influence of geometric and geomaterial heterogeneity, which govern the elastic and creep properties of the cavern (Kumar *et al.,* 2021). Simulations of heterogeneous caverns (i.e., complex cavern shapes and insoluble geomaterials) indicate that the state of stress and deformation locally around the cavern during long-term loading significantly increases as the effects of creep strain are enhanced (Kumar *et al.,* 2021 and Kumar & Hajibeygi, 2022). Furthermore, solution-precipitation creep can influence nonlinear deformation of a cavern and surrounding host rock (Kumar & Hajibeygi, 2022). It has been shown through finite element modelling of a cavern situated in a homogeneous halite formation with a single carnallite interbed that a deviatoric stress threshold develops. The carnallite layer displays much higher horizontal deformation generated by linear pressure solution creep (+ dislocation solution) compared to a cavern situated in pure halite (Kumar & Hajibeygi, 2022). This highlights the importance of incorporating localised pressure solution in the geological domain when modelling the geomechanics of a salt cavern.

In regions of salt where anisotropic stress conditions exist, a loss of gas tightness may occur where the connectivity of pore space results in the generation of interconnected crack openings (Minkley *et al.,* 2015). This can lead to pressure induced openings, loss of the energy vector and deteriorate cavern wall integrity. Furthermore, caverns located near the salt edge of diapiric structures, are likely to experience anisotropic stress conditions in the form of shear zones and melanges, where increased slip and salt flow threaten the security of the stored energy vector, further justifying the 500 m buffer zone from the edge of diapiric salt structures (Kupfer *et al.*, 1998; Evans, 2007 and Caglayan *et al.,* 2020). The general design and related issues that need to be addressed have been summarised in Fig. 5. Note that these might be dictated from local legislation or 'best of practice' codes.

### 3.4. *Site screening, ranking and selection:*

This study took inspiration and adopted a similar methodology developed by Chadwick *et al.* (2008) for ranking saline aquifers for geological $CO_2$ storage. With consideration to the concept of a geological barrier (Raith *et al.,* 2022) the identification, selection, and comparison of key geological indicators, for the optimisation of cavern development in localities suitable for hydrogen storage are stated in Table 3. The values shown are based upon the cavern design established in Section *General*

*cavern design demands* and Section *Salt cavern hydrogen capacity calculations*, determined from the cited literature. A traffic light ranking system was implemented for a more critical refinement of the criterial subgroups, which allows for the possibility of ranking each potential storage site against each other (Tables 3 and 4) (Raith *et al.,* 2022). These values provide a crucial and practical criteria framework for future projects to implement and adapt accordingly for their selected cavern design.

The wells deemed suitable sites for the development of offshore salt caverns and considered to obtain the most reliable sources of information assessed, in agreement with general cavern design demands are presented in Table 4.

3.5. *Salt cavern hydrogen capacity calculations:*

Following the identification of the optimal cavern storage locations, a distribution analysis was performed across the refined eligible areas of selected salt domains to estimate the maximum number of caverns possible within each locality, based on engineering parameters to define and optimise the spacing between caverns (Fig. 5 and Table 2), and refined using the process stated in Section *Regional storage volume corrections*.

Calculations were carried out to determine the total storage potential by considering the hydrogen energy storage capacity, given the appropriate pressure and temperature conditions.

Cavern size is primarily based upon the available salt formation thickness and for this study two cavern configurations utilising the cylindrical-shape design (Fig. 5) were investigated for storage estimations:

- Cavern A with total volume of 500,000 $m^3$ and height of 120 m; and
- Cavern B with total volume of 750,000 $m^3$ and height of 300 m.

Cavern type A and B were selected to reflect the variability of salt thicknesses between domains of bedded and diapiric salt. These cavern sizes are justifiable by operational large-scale hydrogen storage facilities such as the Clemens Dome (580,000 $m^3$; 92 $GWh_{H2}$), Moss Bluff (566,000 $m^3$; 120 $GWh_{H2}$), and Spindletop (906,000 $m^3$; >120 $GWh_{H2}$) sites situated in domal salt structures, USA (Czapowski & Tarkowski, 2018 and Hévin, 2019).

By definition, the cavern's 'total volume' corresponds to the volume of the rock mechanical envelope used for the geomechanical design of the cavern employed for the calculation of the stresses and the displacements around the cavern (including the cavern's sump volume). The 'last cemented casing shoe' (LCCS) is the bottom end or lowermost position of the last cemented string of casing placed in the well inside the intermediate casing and used to flow hydrogen into and out of the well. The section of the wellbore of the cavern, known as 'cavern neck', begins directly beneath the LCCS and ends at the cavern roof (Fig. 5). The height of the cavern neck, which is left uncased as a virgin borehole or minimally washed borehole, determines the depth of the LCCS for a given cavern roof depth. Typically, the neck extends below the LCCS to the cavern roof for a sufficient distance below the end of the casing to prevent roof strains from affecting the integrity of the cemented casing.

The temperature ($T_{LCCS}$) at the depth $z_{LCCS}$ which corresponds to the cavern's LCCS (measured from the seabed level) is expressed in K and calculated as:

Eqn. 1. $$T_{LCCS} = 282.15 + \alpha \times z_{LCCS}$$

where $\alpha$ is the geothermal gradient [°C/m]

The temperature gradient was adapted from Caglayan *et al.* (2020) by employing an approximate North Sea geothermal gradient $\alpha$ equal to 0.031°C/m (Harper, 1971), which is in agreement with publicly accessible North Sea geothermal catalogues of the wells investigated in this study (Table 4), and an average seabed temperature of 9°C (equal to 282.15 K) which is taken to represent the mean summer and winter temperature.

The average temperature of the hydrogen stored in a salt cavern is assumed to be the same as the surrounding host rocksalt (Caglayan *et al.*, 2020). Moreover, the average temperature ($\underline{T_{cav}}$) of the hydrogen at the cavern's mid-height, expressed in K, is calculated using Equation 2 whereby the depth to the cavern roof ($z$), measured from the seabed level, and the cavern height ($h_{\text{cav}}$) are expressed in m.

Eqn. 2. $$\underline{T_{cav}} = 282.15 + 0.031\ (z + h_{cav} / 2)$$

The geostatic vertical stress ($\sigma_v$) at the depth that corresponds to the cavern's LCCS, as shown in Equation 3 and expressed in bar, is a function of:

- the lithostatic gradient of 0.225 bar/m, typically observed in salt formations (Bérest *et al.*, 2020),
- the North Sea seabed pressure (5 bar), and
- the LCCS depth $z_{LCCS}$.

This is an adaptation from the Caglayan *et al.* (2020) methodology, tailored specifically to the studied geological setting.

Eqn. 3. $$\sigma_v = 5 + 0.225 \times z_{LCCS}$$

The 'cavern free volume' is the volume of the cavern that corresponds to the geometrical volume of the cavern, developed during the solution mining process, minus the space occupied by the insolubles and any residual brine that typically occupy the cavern's sump. Hydrogen can be stored in the 'cavern free volume'. By definition, the 'cushion hydrogen volume' is the hydrogen volume needed as permanent storage inventory in the cavern for storage management purposes. It is required for maintaining a suitable minimum storage pressure to adequately support the cavern roof and walls and for delivering hydrogen in accordance with a required withdrawal profile. The 'working hydrogen volume' corresponds to the volume of gas in the cavern above the designed level of cushion hydrogen volume, which can be withdrawn/injected as a reaction to the energy supply and demand profiles of the grid, which are subject to legal and technical limitations (pressures, gas velocities, flowrates, etc.). The availability of working hydrogen volume depends on a number of parameters, such as: the cavern's free volume, the average cavern depth and the respective hydrogen quantities at different pressures and temperatures.

The thermodynamic hydrogen volume analysis presented in this study, employs static pressure calculations based on the barometric elevation formulae (Berberan-Santos *et al.*, 1997). The analysis requires the knowledge of the hydrogen temperature and pressure at the wellhead, the LCCS and the depth corresponding to the mid-height of the cavern.

The analysis determines the pressures in the wellbore and the cavern by employing separate equations because the dominant modes of pressure calculations are different in these two regions.

The two equations are then interlinked, because the pressure of the hydrogen entering and leaving the cavern is equal to the pressure of the hydrogen leaving or entering the wellbore.

The following two equations are available for computing the static pressure $p_{LCCS}$ at the LCCS and the static pressure $p_{cav}$ at the cavern's mid-height respectively, by employing the barometric formula.

The first barometric formula, which is derived from Equation A13 given in the Appendix, calculates the $p_{LCCS}$ and is based on the assumption that the hydrogen composition is constant while progressing from the wellhead level towards the LCCS depth. The temperature is taken to vary linearly with depth with a slope $\alpha$ (expressed in °C/m) that corresponds to the geothermal gradient:

Eqn. 4.
$$p_{LCCS} = p_{wh} \times \left(\frac{T_{LCCS}}{T_{wh}}\right)^{\left(\frac{g_o \times M_{air} \times SG}{R \times \underline{Z}_c \times \alpha}\right)}$$

where: $p_{wh}$ = pressure at the wellhead [bar]

$T_{LCCS}$ = temperature at the depth that corresponds to the LCCS [K]

$T_{wh}$ = temperature at the wellhead level [K]

$g_o$ = standard gravitational acceleration, 9.80665 [m/s$^2$]

$M_{air}$ = molar mass of air, 0.0289652 [kg/mole]

$SG$ = specific gravity of hydrogen, 0.0696

$R$ = universal gas constant equal to 8.3144621 [J/(mol·K)]

$\underline{Z}_c$ = average compressibility factor of the hydrogen column between wellhead and LCCS

$\alpha$ = geothermal gradient equal to 0.031 [°C/m]

The second barometric formula, which is derived from Equation A15 given in the Appendix, employs the $p_{LCCS}$ as input and calculates the $p_{cav}$ by assuming that the hydrogen composition and the temperature remain constant while progressing from the LCCS towards the cavern's mid-height depth:

Eqn. 5.
$$p_{cav} = p_{LCCS} \times e^{\left(\frac{g_o \times M_{air} \times SG \times dh}{R \times \underline{T}_{cav} \times \underline{Z}_{cav}}\right)}$$

where: $dh$ = vertical distance between LCCS and the cavern's mid-height [m]

$\underline{T}_{cav}$ = average temperature in cavern, taken at mid-height [K]

$\underline{Z}_{cav}$ = average compressibility factor of the hydrogen at the cavern's mid-height

By employing the gas law equation for real gases, as specified by Equation A3 in the Appendix, the basic equation that determines the amount of hydrogen mass in the cavern is given by:

Eqn. 6. $$n_h = \frac{p_{cav} \times V_{cav}}{\underline{Z}_{cav} \times \underline{T}_{cav} \times R}$$

where:

$n_h$ = total amount of hydrogen mass under consideration [moles]

$V_{cav}$ = cavern free volume [$m^3$]

Moreover, under standard conditions specified accordingly by the British Standards Institution (2005), the relationship given in the Appendix by Equation A3 may be used to calculate the volume of hydrogen as:

Eqn. 7. $$V_{std} = \frac{n_h \times T_{std} \times Z_{std} \times R}{p_{std}}$$

where:

$V_{std}$ = volume of hydrogen at standard conditions (i.e., at 288.15 K and 1.01325 bar)

$p_{std}$ = standard atmospheric pressure, 1.01325 [bar]

$T_{std}$ = standard temperature, 288.15 [K]

$Z_{std}$ = compressibility factor of hydrogen at standard conditions (1.00071305)

By combining Equations 6 and 7, the following relationship for the volume of the hydrogen at standard conditions may be expressed as:

Eqn. 8. $$V_{std} = \left(\frac{p_{cav}}{p_{std}}\right)\left(\frac{T_{std}}{\underline{T}_{cav}}\right)\left(\frac{Z_{std}}{\underline{Z}_{cav}}\right) V_{cav}$$

Therefore, the volume of hydrogen $V_{std}$ at standard conditions in a cavern may be calculated by employing Equation 8 using as input:

- the average hydrogen temperature $\underline{T}_{cav}$ in the cavern,
- the cavern pressure $p_{cav}$,
- the average compressibility factor $\underline{Z}_{cav}$ of the hydrogen in the cavern, and
- the cavern free volume $V_{cav}$.

The cavern free volume $V_{cav}$ used in Equation 8 is typically determined by employing the results of the most recent sonar survey, while considering the likely loss of storage capacity (see Fig. 4) caused by:

- the volumetric creep closure that potentially occurred since the execution of the sonar survey,
- the volume reduction caused by the insolubles and remnants of brine that accumulate in the cavern's sump, and
- any unplanned construction circumstances during the solution mining of the cavern.

The $V_{cav}$ is often assumed to be 70% of the target cavern total volume, which is typically derived by employing geomechanical criteria (Caglayan *et al.*, 2020). Consequently, the free volume of the two caverns that are investigated in this study is taken as:

- Cavern A – 350,000 $m^3$ = 0.7 × 500,000 $m^3$, and
- Cavern B – 525,000 $m^3$ = 0.7 × 750,000 $m^3$.

The gas compressibility factor *Z*, used in Equation 8, is a dimensionless quantity and is defined as the ratio of the actual volume of n-moles of a gas at *T* and *p* to the ideal volume of the same number of moles at the same *T* and *p*. The hydrogen compressibility factor depends on the pressure *p* and temperature *T*. Fig. 6 shows the variation, with pressure and temperature, of the compressibility factor *Z* for pure hydrogen.

The compressibility factor $\underline{Z_c}$ and the pressure value $p_{LCCS}$ in Equation 4 are determined iteratively, because both parameters are firstly unknown and secondly mutually dependent. Similarly, the compressibility factor $\underline{Z_{cav}}$ and the pressure value $p_{cav}$ in Equation 5 are also found iteratively since both parameters are firstly unknown and secondly mutually dependent.

The compressibility factor for pure hydrogen has been calculated in this study as a function of pressure and temperature by employing the polynomial fitting approach originally developed by Zheng *et al.* (2016).

In this study an assumption is made that 100% pure hydrogen will be stored in the investigated caverns, as there exist storage projects where 95% pure hydrogen is stored in salt caverns (Uliasz-Misiak *et al.*, 2021), eg., UK (Teesside), USA (Clemens, Moss Bluff and Spindletop) and Russia.

The geometrical data employed in the thermodynamic analyses carried out for caverns A and B are summarised in Table 5. The depth of cavern roof from seabed is an average depth of each locality which utilised cavern A or B type design.

Due to geomechanical safety concerns, minimum and maximum hydrogen operational pressures are limited, respectively, to 24% and 80% of the $\sigma_v$ at the depth that corresponds to the cavern's LCCS (Ozarslan, 2012 and Stolzenburg *et al.*, 2014). The lower pressure limit is implemented to maintain cavern stability and sustain hydrogen injection and withdrawal (Wang *et al.*, 2015b), while the maximum hydrogen operation pressure restrictions ensure that the surrounding rock mass remains tight, not only in a structural sense but also, in terms of controlling the potential infiltration of small hydrogen volumes into the salt mass (Brouard *et al.*, 2007).

Furthermore, the assumptions used while undertaking the thermodynamic analyses concerning the hydrogen capacity of the two modelled caverns are summarised in Table 6.

The storage capacity of the salt cavern was determined by using the lower heating volume of the working gas. The lower heating value (also known as net calorific value) of a fuel is defined as the amount of heat released by combusting a specified quantity (initially at 25°C) and returning the temperature of the combustion products to 150°C, which assumes the latent heat of vaporisation of water in the reaction products is not recovered. In converting the hydrogen volume in the cavern, a lower heating value of 3.065 -$kWh_{H2}/Sm^3$ was employed accordingly (Schiro *et al.*, 2019). The hydrogen energy storage capacity estimates were then converted to energy density, calculated by dividing the cavern energy capacity by its free volume, directly linked to different cavern depths

which have a unique temperature and pressure and as such hydrogen energy density. This is strongly related to deeper caverns being able to accommodate a larger amount of working hydrogen. Figure 7 highlights the effects of pressure-temperature on the density of hydrogen, which subsequently affects the energy capacity of the cavern.

The results of the computations for the hydrogen energy stored in caverns A and B, based on the cavern volumes that were calculated using Equation 8, are presented in Table 7.

### 3.6. *Regional storage volume corrections:*

Had our search area been site specific for the development of a single offshore cavern storage site, cavern placement and design (i.e., depth, location, volume and shape) would be optimised according to the available data and storage requirements. A site-specific GAP analysis and identification of additional site investigations would be required. This regional study experienced uncertainties that are a result of the vast area, and the variability in data density of the publicly available datasets. Figure 10, identifies the investigated study area and the borders of this study, highlighting the limited number of available borehole data in salt domains which are considered to be the most reliable sources of information assessed, and are in agreement with the cavern depth ranges stated in Section *General cavern design demands*.

Regional storage estimates were first calculated based on salt volumes identified from seismic data. To reduce uncertainty and obtain more representative hydrogen storage capacity estimates, the following refinement process was applied to determine the total number of potential salt caverns:

- In diapiric salt domains a 500 m buffer zone from the edge of the salt structure was implemented to minimise the risk of encountering rip-up clasts picked up as the salt diapirically penetrated the overlying sediments. The latter ensures that salt cavern development is contained in salts closer to the centre of the salt structure that have a higher likelihood of being homogeneous (refer to Section *Case study – Audrey Salt Wall*). Furthermore, caverns are not considered in areas where salt overhangs or wings exist, created during diapiric flow.
- Using the seismic data and accounting for the 500 m buffer zone a first order refinement of the number of type A and B caverns were mapped into the identified salt domain (diapiric or bedded).
- The storage potential estimate was then conservatively constrained to salt areas suitable for cavern development according to seismic data, which also had at least one borehole penetrating the salt strata. The latter was important since, as discussed previously, borehole data provide the highest data confidence on the salt suitability. This significantly reduced the total number of caverns in the investigated region as boreholes are infrequent in this area. Storage potential was evaluated on a well-by-well basis, based on a more detailed evaluation of the salt structure improving the ‘degree of confidence’ to which the borehole data can be extrapolated.

Therefore, a more representative and conservative number of caverns was determined for that entire salt domain, dependent on factors such as:

  - limitations to seismic datasets (refer to Section *Datasets utilised*);
  - number of exploratory/production borehole datasets;

- degree of salt mobility;
- borehole location within the structure; and
- crucially the interpreted geology at each location.

This ensured cavern placement in theoretically optimal locations suitable for their development.

- In areas of interpreted salt (Figs. 10 and 11), where exploratory/production borehole datasets were not available and seismic data formed the basis of interpretation, a geological uncertainty factor of 50% was applied to the cavern number value (Fichtner, 2014 and Caglayan *et al.,* 2020).

For this reason, in areas where reduced salt volume and lithological variations occur (i.e., bedded salt domains), where there is commonly insufficient salt thicknesses for the development of the larger type B cavern design, the smaller type A cavern design was used (refer to Table 5). As noted in the beginning of this section, the positioning and design of caverns could be further optimised.

The total resulting number of type A caverns, within the investigated regional bedded salt domains of the SNS, estimated from seismic data only, in agreement with cavern spacing values and geospatial exclusions, was determined to be 340. Applying the refinement process described in the bullet points above, the total number of type A caverns within the SNS was determined to be 85. Similarly, in locations where large salt volumes exist (i.e., within the diapiric salt domains), the larger type B cavern design was utilised. The total resulting number of type B caverns within the investigated regional diapiric salt domains of the SNS, estimated from seismic data only, in agreement with cavern spacing values and geospatial exclusions, was determined to be 1,145. As before applying the refinement process, the total number of type B caverns within the SNS was determined to be 195.

These discussed values provide a range for the estimated hydrogen storage potential of the SNS in both bedded and diapiric salt filtered by reducing geological subsurface uncertainty. Furthermore, the difference between the number of caverns determined from seismic data and the number of caverns when refined and tied to borehole data highlight the requirement for further ground investigations tailored for salt cavern exploration to reduce the uncertainty in extrapolating existing datasets, consequently improving storage capacity estimations. The caverns in the two groups, which are represented by cavern A and B type, which reflect the bedded and diapiric salt deposits respectively have been analysed by using the same respective depth and volumes shown in Table 5. Therefore, the potential hydrogen storage capacity from the SNS bedded and diapiric salt domains is in the range of 10 $TWh_{H2}$ to 41 $TWh_{H2}$, and 43 $TWh_{H2}$ to 251 $TWh_{H2}$, respectively.

These calculations should be regarded as a first order indicator of the suitability and potential of a hydrogen storage facility. Site specific investigations will always require detailed data collection and further ground investigations to reduce uncertainty within the data.

### 3.7. *Case study – Audrey Salt Wall:*

One of the largest diapiric salt structures present in the SNS is the Audrey Salt Wall (Figs. 8, 10 and 11), a ~3 km high wall of Permian salt, which has ruptured the overburden and migrated almost to the seabed, forming a broadly linear feature >40 kilometres in length, in parallel to the regional structural trend of the basin (N/NW-S/SE) (Williams *et al.*, 2015). Such extensive salt mobility has resulted in thick vertical accumulations of halite dominated columns forming the core of the salt wall. Based on interpreted well data, the Stassfurt and Leine formations form the main halite sequence of the Audrey Salt Wall core which contains varying amounts of K-Mg salts (Figs. 1 and 8).

K-Mg salts can lead to preferential dissolution influencing the shape of the cavern, as well as having greater creep rates leading to increased cavern convergence and were therefore avoided if possible, during cavern placement (Rowan *et al.,* 2019).

The methodology developed in Fig. 3 was adopted for the investigation of the Audrey Salt Wall, as presented in Fig. 9. Future site-specific investigations should consider the utilisation of existing and future infrastructure as well as producing detailed financial and risk evaluations (refer to Fig. 3).

Thin stringers and/or rafts of non-salt interlayers are more commonly present near the unconsolidated/melange zone at the flanks of the Audrey Salt Wall (Kupfer *et al.,* 1998; Looff, *et al.*, 2003 and Evans*,* 2007). These zones are characterised by sheared and distorted complexes in numerous discrete shear zones. However, from the seismic dataset available, flank resolution of the salt body has restricted resolution, ultimately controlling the degree of confidence in cavern placement. This seismic characteristic indicates a thick zone of disturbed salt, known as an edge anomalous zone, forming in the salt body near the periphery of the salt mass (Looff, *et al.*, 2003). Therefore, without a greater number of boreholes penetrating this region caverns cannot be confidently placed in this edge anomalous zone.

The thickness of this zone will be salt structure specific; dependent on salt thickness, salt structure geometry, and the presence of large stringers (± rafts) being present. Where borehole data was available near the salt edge, even if they did not penetrate the salt or were in the immediate vicinity of the salt, they were used to help constrain the placement and clarify the 'degree of uncertainty' in the positioning of the salt edge.

Due to the sheer scale of the Audrey Salt Wall, the 500 m buffer distance applied has minor significance compared to the total number of potential caverns that can be emplaced in this structure. To minimise drilling risks and to ensure that the target salt deposit is reached, salt cavern locations should be targeted near the core of the diapiric salt structures in addition to further ground investigations being required. This should reduce the risk of drilling into rafts, stringers, and possible shear zones/melanges, where cavern stability will be compromised.

The Audrey Salt Wall in many areas has a non-reflective diapiric core which has been previously interpreted to either represent tightly and intensely folded salt layers (Jones & Davison, 2014), and/or diapirs consisting of pure halite cutting through layers of K/Mg salts, which has been suggest for non-reflective diapirs in Brazil's Santos Basin (Davison *et al.*, 2012). Therefore, seismic opaqueness may indicate localities of more favourable salt compositions for cavern engineering (refer to Section *Datasets utilised*). For the case of the Audrey Salt Wall the boreholes that penetrated these regions tended to consist of favourable salt compositions (Figs. 8, 10 and 11). However, extrapolation of this observation to regions which may be several kilometres away with no borehole data elevates risk and minimises the 'degree of confidence' of cavern placement and cannot be confirmed without further boreholes for verification. In many areas of poor seismic resolution, stringers were commonly the only markers identifiable. They tended to be located nearer the edges of the salt structures consisting of anhydrite-carbonate stringers, and rafts of the overlying sedimentary successions (e.g., clastics). After detailed intra-salt analysis and lithological borehole

verification, cavern placement depths at the investigated borehole localities from this study were determined, allowing for cavern capacity estimations to be thermodynamically derived (refer to Section *Salt cavern hydrogen capacity calculations*).

The refinement methodology stated in Section *Regional storage volume corrections* was applied to the Audrey Salt Wall area using only type B caverns. It was found that the unconstrained number of type B caverns was reduced from 480, to a total of 105. Therefore, the potential hydrogen storage capacity from this single diapiric salt domain was found to be in the range of 23 $TWh_{H2}$ to 105 $TWh_{H2}$.

*4. Results & Discussion:*

The site screening and SNS basin evaluation of the Zechstein Supergroup salt configurations suitability to develop salt caverns has been discussed throughout Section *SNS evaporite deposits* and Section *Methodology & SNS basin evaluation*. The localities investigated in this study are considered to contain suitable salt configurations for the development of underground salt caverns and deemed to have reliable sources of information that indicate there are suitable salt deposits that accommodate general cavern design demands (Tables 2, 3 & 4). The investigated offshore Zechstein Supergroup, therefore, has the potential to be a viable hydrogen storage alternative, and should be considered in future offshore salt cavern storage assessments. As previously discussed, site-specific GAP analysis and further ground investigations are required depending on the investor's requirements. However, the presented methodology highlighted in Fig. 3, along with current publicly available datasets, can help decide whether and where to invest in potential offshore storage sites.

The results of the thermodynamic calculations for the hydrogen energy storage capacity of the investigated caverns have been presented in Section *Salt cavern hydrogen capacity calculations.* Using hydrogen as the energy storage vector and the presented methodology, this study estimated that the overall SNS regional hydrogen storage capacity is in the range of 53 $TWh_{H2}$, if constrained, to 292 $TWh_{H2}$, if all 1,485 caverns are developed based on the assumptions and data limitations discussed in Section *Regional storage volume corrections*. The presented case study, the Audrey Salt Wall was found to have the potential to store approximately half of the estimated total SNS storage capacity determined from this study. The hydrogen storage potential of the UK presented by Caglayan *et al.* (2020) estimated a total of 10,400 $TWh_{H2}$ in both onshore and offshore salt caverns. However, their estimated storage potential is based upon highly idealised salt deposits with uniform depth and thicknesses across the entire deposit. The calculations presented in this study are a more realistic, albeit conservative indication of the vast hydrogen storage potential of the SNS Zechstein deposits. We have shown that the identification of eligible regions and placement of salt caverns is vital for estimating salt cavern quantity and energy capacity, by accounting for geological heterogeneities, thermodynamic properties of the stored hydrogen and cavern design to appropriately estimate cavern energy capacity. Furthermore, the use of locality specific depth and thickness distributions in this study significantly enhances the reliability of the estimated offshore storage capacity potential of the UKCS and should be used as a framework for future studies to further enhance our estimation of UKCS hydrogen storage potential in salt structures. It is also important to highlight that while Fig. 10 indicates that there are extensive salt deposits across the entire SNS, many of these, particularly in the East and Northeast regions are at depths greater than 2,000 m and as such are not suitable for solution mined salt caverns due to increased cavern closure rates, and optimum operating pressures beyond these depths (Plaat, 2009). The storage potential of the SNS may be further reduced when surface and underground barriers that constrain the salt

cavern's construction are considered (Juez-Larré *et al.,* 2019; Tarkowski & Uliasz-Misiak, 2021 and Lankrof *et al.,* 2022). However, the areally extensive and large salt volumes identified in this study at optimal cavern depth ranges located in the SNS (Fig. 10) have the potential to facilitate the development of large numbers of caverns with high upper boundary working hydrogen volumes equivalent to >200 $GWh_H$.

Currently, there are multiple future hydrogen utilisation pathways. The current UK annual electricity consumption is ~300 $TWh_e$ (Evans *et al.*, 2021). If a fully renewable energy system is considered, the UK annual energy demand for power, heat and mobility is expected to increase to ~900 TWh, by 2030 (Blanco & Faaij, 2018). The seasonal hydrogen energy storage demand based on the current methane gas supply UKCS, for a UK domestic heating scenario is estimated to be 78 $TWh_{H2}$ (Mouli-Castillo *et al.,* 2021). To completely replace UK seasonal variations in natural gas consumption the required storage demand increases to 150 $TWh_{H2}$ (Scafidi *et al.,* 2021). By 2035, at least 2 $TWh_{H2}$ of hydrogen storage will be required to provide whole energy system resilience (National Grid Electricity System Operator, 2021). In addition, based on the National Grid Future Energy Scenarios (NGFES) 'system transformation' and 'leading the way' scenarios, they predict that 74 $TWh_{H2}$ to 77 $TWh_{H2}$ of hydrogen storage will be required by 2050 to achieve net zero emission targets (National Grid Electricity System Operator, 2021). The UK's current natural gas storage capacity in caverns has the capability of storing approximately 4.7 $TWh_{H2}$, increasing to a total of 8.5 $TWh_{H2}$ if all undergoing projects are developed (Parkes *et al.,* 2018 and Williams *et al.,* 2022).

The above accentuates both the increase in future hydrogen demand and the storage and supply demand that is required to integrate hydrogen into energy systems. To facilitate this transition large-scale geological storage, such as the proposed salt cavern storage options presented in this study, should provide the fundamental building blocks necessary for a successful energy transition. The storage estimations presented in this study suggest that salt cavern storage on the UKCS, SNS can contribute significantly to the required hydrogen storage, which is essential for a low carbon, net zero future by 2050. Furthermore, the integration of offshore salt cavern hydrogen storage with existing offshore low carbon and carbon mitigating technologies (i.e., offshore wind and carbon sequestration) could transform the UKCS into an integrated, highly efficient synergy system (Williams *et al.,* 2022). This could re-establish the UKCS as a net-energy exporter while importantly transitioning to low carbon technologies.

Concerning the major challenges of drilling and developing offshore salt cavern sites, a study assessing the risks of ultra-deep water salt cavern $CO_2$ storage off the coast of Brazil in the Santos Basin has been conducted (Maia da Costa *et al.,* 2019 and Pestana *et al.,* 2019). A comprehensive preliminary risk analysis was carried out by means of hazard, frequency, cause, and consequence of events. Their analysis found no 'intolerable' technical risks associated with ultra-deep water drilling, cavern development and operation, however like all subsurface exploration there are some associated risks that need to be managed. Furthermore, no technology gaps have been identified that could make the offshore salt cavern storage projects unfeasible (Goulart *et al.*, 2020). Their assessment indicates that the technology to develop offshore salt caverns is ready and can be implemented in the shallower water depths of the SNS. Importantly, the Gateway project in the East Irish Sea had been granted approval for development in 2008 which when coupled with dCarbonX and ESB, as well as Tractebel and partner companies' recent announcements of the world's first offshore hydrogen storage concepts in offshore salt caverns, confirms the reality and feasibility of this the technology (Tractebel, 2021 and ESB, 2021). Generally, any operation conducted offshore

will cost more to develop and operate than its onshore alternative (McCall *et al.,* 2005). However, a report assessing the potential of developing offshore salt caverns to receive ship borne LNG, offshore Louisiana, estimated that offshore caverns are unit cost competitive with onshore tank-based terminals and less expensive than offshore tank-based alternatives (McCall *et al.,* 2005 and Rai, 2007).

Salt caverns are a proven hydrogen storage technology that are safe to operate with a large operational lifespan. An additional advantage is their ability to endure multiple loading and unloading operational cycles. This effectively increases the working gas storage capacity providing demand flexibility for both daily, weekly and seasonal storage (Evans *et al*., 2021). Depending on the applicational demand, supply, and profitability for the energy vector, which is likely to fluctuate significantly on a seasonal timescale, the 'total stored energy per year' estimates could significantly increase if a fast cyclic loading approach is taken in the operation of the salt caverns. This highlights salt caverns' importance to deliverability, due to their flexibility to deliver operational cyclicity. This is evident across the globe, in 2021 salt caverns provided ~8% of the working gas storage capacity, yet contributed 26% of global deliverability from storage facilities (Losson, 2021).

It is acknowledged that a probabilistic approach could have been applied, such as the study conducted by Lankof *et al.* (2022) for the gas cavern storage facility Mogilno located in the Polish Zechstein Basin. It must be noted that despite best efforts to incorporate relevant SNS publicly available data, additional information is needed to reach an acceptable confidence level to decide on which site/s are optimal for developing a hydrogen storage cavern site. As such, utilisation of complex statistical model/s might lead to biased assurance, something that the authors of this study would not be comfortable with. Nevertheless, the presented guidance can be used for such analysis, especially if the area of interest is of similar size to the one examined by Lankof *et al.* (2022), hence smaller to the one investigated in this publication, and if additional information became available.

## 5. *Conclusions:*

This study presented a methodology that employs publicly available datasets for identifying offshore salt cavern locations for the storage of hydrogen, due to the recognition of hydrogen's 'critical' role in decarbonisation projections. This is driven by the versatility of hydrogen to act as an energy carrier, facilitating the decarbonisation of both industrial and domestic energy sources. The proposed step-by-step methodology also allows for estimating the storage potential of such caverns which supports the decision-making process whether to progress with the development of an offshore salt cavern storage facility.

A case study focused on the UKCS area was also presented to demonstrate the potential, strength and weaknesses of the method, and in particular, the Audrey Salt Wall located in the SNS basin. The chosen geological area highlighted the potential and suitability of the vast offshore Permian salt deposits for cavern development.

Currently, there are no active hydrogen storage projects for energy production in the UK, however, based on the published UK decarbonisation roadmaps, accessible large-scale, GW to TW hydrogen storage needs to be secured. The Zechstein Supergroup, UKCS has the potential to deliver the required storage capacities for future hydrogen production and supply networks, with the additional benefit of providing *in situ* storage alternatives for future offshore wind farm projects. Based on this study 53 $TWh_{H2}$ to 292 $TWh_{H2}$ of storage volume could exist in offshore salt caverns which is in

excess of ~70% to ~380% of the required hydrogen storage quoted from NGFES 'leading the way' scenario. For hydrogen to successfully achieve its role in climate-neutral decarbonisation scenarios, geological storage is essential. Hydrogen storage in offshore salt caverns, due to their large storage capacities and versatile operational capabilities, can assist the energy transition and meet Net Zero targets, and therefore, should be strongly considered as a solution to facilitate our energy storage requirements.

*Acknowledgements:*

The authors thank the North Sea Transition Authority for kindly providing the wealth of offshore licence datasets (e.g., PGS SNS MegaSurvey Version 2.0 2016) and the paper contains information provided by the North Sea Transition Authority and/or other third parties. Schlumberger is thanked for providing Petrel 2018 seismic interpretation software under academic licence. KE is supported by funding from the HyStorPor project [grant number EP/S027815/1] and the EU H2020 HyUsPRe project, [Grant agreement ID: 101006632].

*Appendix:* Derivation of thermodynamic static pressure calculations

The equation of hydrostatic equilibrium is used to determine the pressure variation in the cavern's well by employing the following mathematical analysis:

Considering the force balance of the elemental height *dh* of the cylindrical volume of a column of gas, with cross sectional area *A*, density *ρ* and mass *m*, as shown in Fig. A1, the gravitational force (which is calculated by multiplying the mass by the standard gravitational acceleration, $m \times g_o$) must be counterbalanced by the difference in the pressure forces acting on the two faces, hence:

$(p + dp) \times A - m \times g_o = p \times A$ or

$p \times A + dp \times A - m \times g_o = p \times A$ or

$dp \times A - m \times g_o = 0$ or

$dp \times A - (\rho \times dh \times A) \times g_o = 0$ or

$dp - \rho \times dh \times g_o = 0$ or

Eqn. A1. $$dp = \rho \times g_o \times dh$$

The state of the amount of gas in the cylindrical element shown in Fig. A1, is determined by its pressure, volume, and temperature by employing the equation of state that correlates densities of gases to temperatures and pressures.

An equation of state is a thermodynamic equation that describes the state of matter under a given set of physical conditions. One of the simplest equations of state for this purpose is the ideal gas law:

Eqn. A2. $$p \times V = n \times R \times T$$

where:

| | | |
|---|---|---|
| $p$ | = | average pressure of the gas [bar] |
| $V$ | = | total volume of the gas considered [$m^3$] |
| $n$ | = | total amount of substance of gas [moles] |
| $R$ | = | universal gas constant equal to 8.3144621 [J/(mol·K)] |
| $T$ | = | average temperature of gas [K] |

The molecules of an ideal gas are assumed to occupy no space and have no attractions for one another. Real molecules, however, do have finite volumes and they do attract one another; so in real gases the molecules interact and if they are close enough they result in a potential energy contribution. At temperatures near the critical temperature the behaviour of real gases can, even at low pressures, deviate considerably from that of the ideal gas law of Equation A2.

At high pressures a correction of the value calculated using the ideal gas law must be made for all gases, and usually this is done by introducing in Equation A2 the real gas compressibility factor *Z* which results in the real gas equation of state:

Eqn. A3. $$p \times V = Z \times n \times R \times T$$

The compressibility factor *Z* measures the deviation of a gas from its ideal state, while comparison of Equations A2 and A3 indicates that the compressibility factor is equal to 1 in an ideal gas. However, in a real gas, as the pressure increases, *Z* increases to a number larger than one, distorting the ideality. The same is true for when a temperature decreases, as the compressibility factor rises above 1 again as the temperature approaches a smaller number.

How much gas is present in the cylindrical element shown in Fig. A1 may be identified by specifying the mass instead of the total amount of substance of gas (*n*). Therefore, an alternative form of the real gas equation of state (Equation A3) may be useful. The total amount of substance (*n*), in moles, is equal to the mass of the gas (*m*), in kg, divided by the molecular weight of the gas ($M_g$), in kg per mole:

Eqn. A4. $$n = \frac{m}{M_g}$$

By combining Equations A3 and A4 we get:

Eqn. A5. $$p = \frac{m \times R \times T \times Z}{M_g \times V}$$

Moreover, by introducing the gas density as $\rho = m/V$, Equation A5 becomes:

Eqn. A6. $$p = \frac{\rho \times R \times T \times Z}{M_g}$$

Since the molecular weight of the gas ($M_g$) is related to the molecular weight of the air ($M_{air}$) by means of Equation A7:

Eqn. A7. $$M_g = M_{air} \times SG$$

where *SG* is the specific gravity of gas (i.e., the ratio of the gas density to the air density), by substituting Equation A7 into equation A6 we get:

Eqn. A8. $$p = \frac{\rho \times R \times T \times Z}{M_{air} \times SG}$$

Dividing Equation A1 by equation A8 we get:

Eqn. A9. $$\frac{dp}{p} = \frac{g_o \times dh \times M_{air} \times SG}{R \times T \times Z}$$

**Case 1: Temperature varies along gas column**

The temperature $T_L$ at the lower point of a gas column may be estimated by adding the temperature $T_U$ at the upper point of the gas column, to the product of the thermal gradient $\alpha$ with the height $h$ of the gas column:

Eqn. A10. $$T_L = T_U + (\alpha \times h)$$

Differentiating Equation A10 we obtain:

Eqn. A11. $$dT = \alpha \times dh$$

and by setting $Z$ equal to $\underline{Z}$, which is the mean Z value for the column of gas, while substituting Equation A11 into Equation A9 and simplifying we get:

$$\frac{dp}{p} = \frac{g_o \times M_{air} \times SG}{R \times \underline{Z} \times \alpha} \left(\frac{dT}{T}\right)$$

which when integrated results into Equation 12:

Eqn. A12. $$\int_{p_U}^{p_L} \frac{dp}{p} = \frac{g_o \times M_{air} \times SG}{R \times \underline{Z} \times \alpha} \int_{T_U}^{T_L} \frac{dT}{T}$$

where:

$p_L$ = average pressure of the gas at the lower point of a gas column [bar]

$p_U$ = average pressure of the gas at the upper point of a gas column [bar]

In solving the integrals in Equation 12 we get:

$$ln\left(\frac{p_L}{p_U}\right) = \frac{g_o \times M_{air} \times SG}{R \times \underline{Z} \times \alpha} ln\left(\frac{T_L}{T_U}\right)$$

which, by taking anti-logarithms, results into the following equation:

Eqn. A13. $$p_L = p_U \times \left(\frac{T_L}{T_U}\right)^{\frac{g_o \times M_{air} \times SG}{R \times \underline{Z} \times \alpha}}$$

**Case 2: Temperature constant along gas column**

When the temperature is not a function of depth and is assumed to be constant and equal to $\underline{T}$(= mean temperature of gas column), then $Z$ assumes a mean value equal to $\underline{Z}$, and equation A9 becomes:

Eqn. A5. $$\frac{dp}{p} = \frac{g_o \times dh \times M_{air} \times SG}{R \times \underline{T} \times \underline{Z}}$$

which when integrated results into:

$$\int_{p_U}^{p_L} \frac{dp}{p} = \frac{g_o \times M_{air} \times SG}{R \times \underline{T} \times \underline{Z}} \int_{h_U}^{h_L} dh$$

from which we get:

$$ln\left(\frac{p_L}{p_U}\right) = \frac{g_o \times M_{air} \times SG \times (h_U - h_L)}{R \times \underline{T} \times \underline{Z}}$$

which, by taking anti-logarithms, results into the following equation:

Eqn. A15. $$p_L = p_U \times e^{\left(\frac{g_o \times M_{air} \times SG \times \delta h}{R \times \underline{T} \times \underline{Z}}\right)}$$

## References


Abuaisha, M. & Billoiotte, J. 2021. A discussion on hydrogen migration in rock salt for tight underground storage with an insight into a laboratory setup. J. Energy Storage 2021;38:102589. April.

Adam, J., Payne, M., Lashko, E., Lawleere, S., Scarselli, N. & More, S. 2017. Impact of Thin- and Thick-Skinned Salt Tectonics on the Mesozoic Reservoir Potential of the Cleaver Bank High and Broad Fourteen Basin, Dutch Sector, Southern North Sea. Abstract from AAPG International Conference & Exhibition, London, United Kingdom.

Asgari, A., Ramezanzadeh, A., Jalali, S.M.E. & Brouard, B. 2020. Stability analysis of salt cavern gas storage using 2D thermo-hydro- mechanical finite-element software. Journal of Mining & Environment, 11(1):77-97.

Barnett, H., Ireland, M.T. & Acikalin, S. 2021. Assessing the Feasibility of Large-Scale Hydrogen Storage in Salt Caverns on the UKCS Using 3D Seismic Data. In Proceedings of the EGU General Assembly Conference Abstracts, Vienna, Austria, 19–30 April 2021.

Bartholomew, C. H., & Farrauto, R. J. 2006. In Fundamentals of industrial catalytic processes.

Hoboken, New Jersey, USA: John Willey and Sons (Chapter 6).

Berberan-Santos, M.N., Bodunov, E.N. & Pogliani, L. 1997. On the barometric formula, American Journal of Physics, May 1997, 65(5):404-412.

Bérest, P. & Brouard, B. 2003. Safety of salt caverns used for underground gas storage. Oil & Gas Science and Technology, 58:361-384.

Bérest, P. 2011.Thermomechanical aspects of high frequency cycling in salt storage caverns, International Gas Union Research Conference, October, Seoul, South Korea, pp.22.

Bérest, P., Brouard, B., Karimi-Jafari, M. & Réveillère, A. 2020. Maximum admissible pressure in salt caverns used for brine production and hydrocarbon storage, Oil & Gas Science and Technology – Revue d' Institut Français du Pétrole, Energies nouvelles 75(76), https://doi.org/10.2516/ogst/2020086.

Bérest, P., Révillère, A., Evans, D. & Stöwer, M. 2019. Review and analysis of historical leakages from storage salt caverns wells, Oil & Gas Science and Technology-Rev. IFP Energies nouvelles, 74(27), https://doi.org/10.2516/ogst/2018093.

Beutel, T. & Black, S. 2005. Salt deposits and gas cavern storage in the UK with a case study of salt exploration from Cheshire. Oil & Gas European Magazine, 1:31-35.

Blanco, H. & Faaij, A. 2018. A review at the role of storage in energy systems with a focus on power to gas and long-term storage. Renewable and sustainable energy reviews, July 2017, 81:1049-1086. https://doi.org/10.1016/j.rser.2017.07.062.

British Standards Institution 2005. BS EN ISO 13443:2005, Natural gas - Standard reference conditions, pp.20.

Brouard B., Bérest, P. & Karimi-Jafari, M. 2007. Onset of tensile effective stresses in gas storage caverns, Solution Mining Research Institute, Proc. tech. conf., Halifax, 8-10 October 2007, 119-136.

Bruno, M.S. 2005. Geomechanical analysis and design considerations for thin-bedded salt caverns, Final report no. DE-FC26-03NT41813, GTI Contract 8701, Terralog Technologies Inc., Arcadia, CA, USA, pp.142.

Bünger, U., Michalski, J., Crotogino, F., & Kruck, O. 2016. 7 - Large-scale underground storage of hydrogen for the grid integration of renewable energy and other applications. In *Compendium of Hydrogen Energy* (pp. 133-163). Elsevier.

Burliga, S., 2014. Heterogeneity of folding in Zechstein (Upper Permian) salt deposits in the Kłodawa Salt Structure, central Poland. Geological Quarterly, 58 (3): 565–576, doi: 10.7306/gq.1153

Caglayan, D.G., Weber, N., Heinrichs, H.U., Linßen, J., Robinius, M., Kukla, P.A. & Stolten, D. 2020. Technical potential of salt caverns for hydrogen storage in Europe. International Journal of Hydrogen Energy, 45(11):6793-6805, https://doi.org/10.1016/j.ijhydene.2019.12.161.

Cala, M., Cyran, K., Kowalski, M. & Wilkosz, P. 2018. Influence of the anhydrite interbeds on a stability of the storage caverns in the Mechelinki salt deposit (Northern Poland). Archives of Mining Sciences, 63(4):1007-1025, https://doi.org/10.24425/ams.2018.124990.

Cameron, T.D.J., Crosby, A., Balson, P.S., Jeffrey, D.H., Lott, G.K., Bulat, J. & Harrison, D.J. 1992. The geology of the southern North Sea, British Geological Survey, United Kingdom Offshore Regional Report, London, HMSO, pp.170.

Chadwick, A., Arts, R., Bernstone, C., May, F., Thibeau, S. & Zweigel, P. 2008. Best practice for the storage of CO2 in saline aquifers, Observations and guidelines from the SACS and CO2STORE projects, Nottingham, UK, British Geological Survey Occasional Publication 14, pp.267.

Chemia, Z., Schmeling, H. & Koyi, H. 2009. The effect of the salt viscosity on future evolution of the Gorleben salt diapir, Germany. *Tectonophysics* 2009, *473*, 446–456.

Clipsham, W. B., Olafson, D.D., Pratt, B.G. & Steuart, B.A. 1965. Economic Considerations Concerning the use of Salt Caverns for Natural Gas Storage by an Integrated Natural Gas Transmission and Distribution System. 16th Annual Technical Meeting, The Petroleum Society of C.I.M., Calgary, May, 1965.

Committee on Climate Change 2020. The Sixth Carbon Budget: The UK's path to Net Zero, a report to the Secretary of State pursuant to section 34 of the Climate Change Act 2008, December, pp.448.

Crotogino F., Mohmeyer, K.-U. & Scharf R. 2001. Huntorf CAES: More than 20 years of successful operation, Solution Mining Research Institute, Proc. tech. conf., Orlando, Florida, USA, 15-18 April 20, pp.7.

Cyran, K. 2020. Insight into a shape of salt storage caverns. *Arch. Min. Sci.* 65 (2), 363-398, doi:10.24425//ams.2020.133198.

Czapowski, G. & Tarkowski, R. 2018. Geology of selected salt domes in Poland and their usefulness in constructing hydrogen storage caverns. Biuletyn Państwowego Instyutu Geologicznego, (472), 53-81.

Davison, I., Anderson, L. & Nuttall, P. 2012, Salt deposition, loading and gravity drainage in the Campos and Santos Salt Basins, Salt tectonics, sediments and prospectivity, Geological Society, London, Special Publications, 363:159-174, https://doi.org/10.1144/SP363.8.

Davison, I., Jones, I. F. & Waltham, D. 2013. Seismic Imaging of Salt Diapirs: Problems and Pitfalls. Thirteenth International Congress of the Brazilian Geophysical Society. Doi: 10.1190/sbgf2013-274.

Duffy, O.B., Hudec, M.R., Peel, F., Apps, G., Bump, A., Moscardelli, L., Dooley, T.P., Bhattacharya, S., Wisian, K. & Shuster, M.W. 2022. The Role of Salt Tectonics in the Energy Transition: An Overview and Future Challenges. Under peer-review. https://doi.org/10.31223/X5363J.

Duguid, C. & Underhill, J.R., 2010. Geological controls on upper Permian Plattendolomit Formation reservoir prospectivity, Wissey field, UK Southern North Sea. Pet. Geosci. 16, 331–348. https://doi.org/10.1144/1354-0793/10-021.

Elam, S. 2007. First Gas after 40 Years – The Geophysical Challenges of the Saturn Gas Complex. AAPG 2007 Annual Convention, Long Beach, California, April 1-4, 2007.

Energy Technologies Institute 2015. Hydrogen, The role of hydrogen storage in a clean responsive power system. http://www.Eti.Co.Uk/Wp-Content/Uploads/2015/05/3380-ETI-Hydrogen-Insights.

ESB 2021. ESB and dCarbonX to partner on green hydrogen storage development. https://esb.ie/media-centre-news/press-releases/article/2021/05/26/esb-and-dcarbonx-to-partner-on-green-hydrogen-storage-development

Evans, D.J., Parkes, D., Dooner, M., Williamson, P., Williams, J., Busby, J., He, W., Wang, J. & Garvey, S. 2021. Salt cavern exergy storage capacity potential of UK massively bedded halites, Using compressed air energy storage (CAES). Appl. Sci. 2021, 11(4728), https://doi.org/ 10.3390/app11114728.

Evans, D.J. & Holloway, S. 2009. A review of onshore UK salt deposits and their potential for underground gas storage. in D.J. Evans & R.A. Chadwick (eds) Underground gas storage: Worldwide experiences and future development in the UK and Europe. Geological Society, London, Special Publications, 313:39-80.

Evans, D.J. 2007. An appraisal of Underground Gas Storage technologies and incidents, for the development of risk assessment methodology. *British Geological Survey Open Report*, OR/07/023. 287pp.

Fichtner, GmbH 2014. Erstellung eines Entwicklungskonzeptes Energiespeicher in Niedersachsen, report no. 7983P01/FICHT-12919463-v19 for Innovationszentrum Niedersachsen GmbH, pp.197

Geluk, M.C. 2005. Stratigraphy and tectonics of Permo-Triassic Basins in the Netherlands and surrounding areas, PhD thesis, Utrecht University, pp.171.

Géostock. 2007. AGA - IGU Meeting. Dallas, April 24th, 2007.

Gevantman, L.H. (ed) 1981. Physical properties data for rock salt, NBS monograph 167, U.S. Department of Commerce, National Bureau of Standards, Washington, D.C. 20234, pp.300.

Glennie, K.W. 1990. Introduction to the petroleum geology of the North Sea, Blackwell Scientific Publications, Oxford, pp.402.

Goulart, M.B.R., Maia de Costa, P.V., Maia de Costa, A., Miranda, A.C.O., Mendes, A.B., Ebecken, N.F.F., Meneghini, J.R., Nishimoto, K., & Assi, G.R.S. 2020. Technology readiness assessment of ultra-deep salt caverns for carbon capture and storage in Brazil: International Journal of Greenhouse Gas Control, v. 99, August, p.103083.

Grant, R.J., Underhill, J.R., Hernández-Casado, J., Barker, S.M. & Jamieson, R.J. 2019. Upper Permian Zechstein Supergroup carbonate-evaporite platform palaeomorphology in the UK Southern North Sea, Marine and Petroleum Geology, 100:1(484-518), https://doi.org/10.1016/j.marpetgeo.2017.11.029.

Hamilton, W.N. 1971. Salt in east-central Alberta. Research Council of Alberta, RCA/AGS Bulletin 29, pp.65.

Haimson, B.C., 1974, Mechanical behavior of rock under cyclic loading. Proceedings of the 3rd Congress of the International Society for Rock Mechanics, Part A. Advances in Rock Mechanics: Report of Current Research; Sept 1-7, 1974; Denver, National Academy of Sciences, Washington, D.C., p. 373-387.

Harding, R., & Huuse, M. 2015. Salt on the move: Multi stage evolution of salt diapirs in the Netherlands North Sea. *Marine and Petroleum Geology, 61*, 39-55.

Harper, M.L. 1971. Approximate geothermal gradients in the North Sea Basin, Nature, 26 March, 230:235-236.

Hassanpouryouzband, A., Joonaki, E., Edlmann, K. & Haszeldine, R.S. 2021. Offshore geological storage of hydrogen: Is this our best option to achieve net-zero? ACS Energy Letters 6(6):2181-2186, https://doi.org/10.1021/acsenergylett.1c00845.

He, W., Luo, X., Evans, D., Busby, J., Garvey, S., Parkes, D., & Wang, J. 2017. Exergy storage of compressed air in cavern and cavern volume estimation of the large-scale compressed air energy storage system. Applied Energy, 208, 745-757.

Hévin, G. 2019. Underground storage of hydrogen in salt caverns. European workshop on underground energy storage. November 7-8th, 2019, Paris.

HM Government 2021. UK hydrogen strategy, Command Paper 475, 17 August, pp.121.

Howard, A.S., Warrington, G., Carney, J.N., Ambrose, K., Young, S.R., Pharaoh, T.C. and Cheney, C.S. 2009. Geology of the Nottingham District. Memoir of the British Geological Survey, Sheet 126 (England and Wales).

Jackson, M., Cornelius, R.R., Craig, C.H., Gansser, A., Stöcklin, J. & Talbot, C.J. 1990. Salt Diapirs of the Great Kavir, Central Iran. *Mem. Geol. Soc. Am.* 1990, *177*, 1–139.

Jackson, C.A.L., Jackson, M.P.A., Hudec, M.R. & Rodriguez C.R. 2015. Enigmatic structures within salt walls of the Santos Basin-Part 1: Geometry and kinematics from 3D seismic reflection and well data, Journal of Structural Geology 75:135-162.

Jackson, M. & Hudec, M. 2017. Evaporites and their deposition, in Salt Tectonics: Principles and practice Cambridge, Cambridge University Press, p.28-60. https://doi.org/10.1017/9781139003988.005.

Jones, I.F. & Davison, I. 2014. Seismic imaging in and around salt bodies. Interpretation, 2(4), SL1–SL20, https://doi.org/10.1190/INT-2014-0033.1.

Juez-Larré J., van Gessel S., Dalman R., Remmelts G. & Groenenberg, R. 2019. Assessment of underground energy storage potential to support the energy transition in the Netherlands. First Break 2019;37(7):57–66.

Kumar, R., Makhmutov, A., Spiers, C. & Hajibeygi, H. 2021. Geomechanical simulation of energy storage in salt formations. *Scientific Reports, 11*(1), 19640.

Kumar, R., & Hajibeygi, H. 2022. Influence of pressure solution and evaporate heterogeneity on the geo-mechanical behavior of salt caverns. In *The Mechanical Behavior of Salt X* (1st ed., pp. 407-420). CRC Press.

Kupfer, D.H., Lock, B.E. & Schank, P.R. 1998. Anomalous zones within the salt at Weeks Island, Louisiana, Gulf Coast Assoc. of Geol. Soc. Trans., XLVIII:181-192.

Landinger, H. & Crotogino, F. 2007. The role of large-scale hydrogen storage for future renewable energy utilisation, Second Int. Renew. Energy storage Conf. (IRES II) (2007).

Landrø, M., Puigdefabregas, C. & Arntsen, B. 2011. Anisotropy in the salt outcrop at Cardona, Catalonia-Implications for seismic imaging: First Break, 29:41–45, https://doi.org/10.3997/1365-2397.2011022.

Lankof, L., Urbańczyk, K., & Tarkowski, R. 2022. Assessment of the potential for underground hydrogen storage in salt domes. *Renewable & Sustainable Energy Reviews, 160*, 112309.

Li, J., Tang, Y., Shi, X., Xu, W., & Yang, C. 2019. Modeling the construction of energy storage salt caverns in bedded salt, Applied Energy, 255, December, article 113866, https://doi.org/10.1016/j.apenergy.2019.113866.

Li, S., Urai, J. 2016. Numerical modelling of gravitational sinking of anhydrite stringers in salt (at rest). Bollettino di Geofisica Teorica ed Applicata 57(3):233-246.

Li, W., Miao, X., & Yang, C. 2020. Failure analysis for gas storage salt cavern by thermo-mechanical modelling considering rock salt creep. Journal of Energy Storage, 32, October, 102004. https://doi.org/10.1016/j.est.2020.102004.

Li, Z., Go, P., Han, R. & Sun, H. 2018. Current status and development trend of wind power generation-based hydrogen production technology, Energy Exploration and Exploitation, 2018, https://doi.org/10.1177/0144598718787294

Looff, K., Duffield, J. & Looff, K. 2003. Edge of salt definition for salt domes and other deformed salt structures – Geologic and geophysical considerations. Solution Mining Research Institute, Proc. tech. conf., Houston, Texas, USA, 27-30 April, pp.20.

Losson, L. 2021. Underground Gas Storage in the World - 2021 Status. CEDIGAZ Insights, Underground Gas Storage, 3 December 2021. https://www.cedigaz.org/underground-gas-storage-in-the-world-2021-status.

Lux, K.-H. 2009. Design of salt caverns for the storage of natural gas, crude oil and compressed air: Geomechanical aspects of construction, operation and abandonment, in D.J. Evans & R.A. Chadwick (eds), Underground gas storage: Worldwide experiences and future development in the UK and Europe, The Geological Society, London, Special Publications, 313: 93–128.

Ma, X., Xu, Z., Chen, L., & Shi, X. 2021. Creep deformation analysis of gas storage in salt caverns. *International Journal of Rock Mechanics and Mining Sciences (Oxford, England : 1997), 139*, 104635.

MacDonald, M. 2014. Preesall underground gas storage facility: Geological summary report for Halite Energy Group: Altrincham, UK, pp.169.

Maia da Costa, A., Costa, P.V.M., Miranda, A.C.O., Goulart, M.B.R., Udebhulu, O.D., Ebecken, N.F., Azevedo, R.C., de Eston, S.M., de Tomi, G., Mendes, A.B., Meneghini, J.R., Nishimoto, K.,

Sampaio, C.M., Brandão, C. & Breda, A. 2019. Experimental salt cavern in offshore ultra-deep water and well design evaluation for CO2 abatement. *Int. J. Min. Sci. Technol.* **2019**, *29*, 641–656.

Malaguti, R., Allen, M., Litvin, A. & Gregory, C. 2001. Sub-salt imaging using 3D pre-stack depth migration in the UK Southern North Sea - a case history, European Association of Geoscientists & Engineers, First Break, 19(5), May, https://doi.org/10.1046/j.0263-5046.2001.00157.x.

Maystrenko, Y.P., Bayer, U. & Scheck-Wenderoth, M., 2012. Regional-scale structural role of Permian salt within the Central European Basin System, in G.I. Alsop, S.G. Archer, A.J. Hartley, N.T. Grant, & R. Hodgkinson (eds), Salt tectonics, sediments and prospectivity, Geological Society, London, Special Publications, 363:409-430, https://doi.org/10.1144/ SP363.19.

Maystrenko, Y.P., Bayer, U. & Scheck-Wenderoth, M. 2013. Salt as a 3D element in structural modelling - Example from the Central European Basin System. Tectonophysics, 591:62-82, https://doi.org/10.1016/j.tecto.2012.06.030.

McCall, M.M., Davis, J.F. & Taylor, C. 2005. Offshore salt-cavern-based LNG receiving terminal, paper presented at the International Petroleum Technology Conference, Doha, Qatar, November, https://doi.org/10.2523/IPTC-10694-MS.

Minkley, W., Knauth, M., Fabig, T. & Farag, N. 2015. Stability and integrity of salt caverns under consideration of hydro-mechanical loading. In Proceedings of the Seventh Conference on the Mechanical Behavior of Salt, Paris 16-19 April 2012, eds. P. Bérest et al., 217-227. London: Taylor & Francis

Mouli-Castillo, J., Heinemann, N. & Edlmann, K. 2021. Mapping geological hydrogen storage capacity and regional heating demands: An applied UK case study, Applied Energy, 283(116348), pp.24, https://doi.org/10.1016/j.apenergy.2020.116348.

National Grid Electricity System Operator Ltd 2021. Future energy scenarios, July, pp.298.

Ozarslan, A. 2012. Large-scale hydrogen energy storage in salt caverns, International Journal of Hydrogen Energy 37(19):14265-14277.

Panfilov, M. 2015. Underground and pipeline hydrogen storage, in R.B. Gupta (ed), Compendium of hydrogen energy, Elsevier, 4:92-116.

Parkes, D., Evans, D., Williamson, P., & Williams, J. 2018. Estimating available salt volume for potential CAES development: A case study using the Northwich Halite of the Cheshire Basin. Journal of Energy Storage, 18:50-61.

Passaris, E. Slingsby, J., Yfantis, G. 2018. The rationality of employing a de-pressurisation rate limit to regulate the export capability of gas storage salt caverns. Solution Mining Research Institute Fall 2018 Conference. Belfast, Northern Ireland, UK, 24-25 September 2018.

Passaris, E. & Wood, J. 2019. Project Islandmagee Energy – The natural gas storage facility in Northern Ireland, Solution Mining Research Institute; Proc. tech. conf., New Orleans, Louisiana, USA, 8-9 April, 155-164.

Peryt, T.M., Geluk, M.C., Mathiesen, A., Paul, J. & Smith, K. 2010. Zechstein. in: J.C. Doornebal and A.G. Stevenson (eds), Petroleum Geological Atlas of the Southern Permian Basin Area. EAGE Publications b.v, Houten, p.123-147.

Pestana, M.A., Morais, C.H.B., Maia da Costa, A., Brandão, C. & Martins, M.R. 2019. Risk assessment in offshore salt caverns to store $CO_2$. Proceedings of the ASME 2019 38th

International conference on Ocean, Offshore and Arctic Engineering. June 9-14, 2019, Glasgow, Scotland, UK.

Petroleum Geo-Services Reservoir 2016. Southern North Sea MegaSurvey. Report 01.1343 & 04.1600/r2, July 2016.

Pichat, A. 2022. Stratigraphy, Paleogeography and Depositional Setting of the K–Mg Salts in the Zechstein Group of Netherlands—Implications for the Development of Salt Caverns. *Minerals (Basel), 12*(4), 486.

Plaat, H. 2009. Underground gas storage: Why and how. in D.J. Evans, and R.A. Chadwick (eds) Underground gas storage: Worldwide experiences and future development in the UK and Europe. Geological Society, London, Special Publications, 313:25-37.

Portarapillo, M. & Di Benedetto, A. 2021. Risk assessment of the large-scale hydrogen storage in salt caverns. Energies, 14(2856). https://doi.org/10.3390/en14102856.

Rai, S. 2007. Offshore LNG Technology: A Comparative Study of Conventional and Futuristic Salt-Cavern-Based LNG Receiving Terminals. Paper presented at the Latin American & Caribbean Petroleum Engineering Conference, Buenos Aires, Argentina, April 2007. doi: https://doi.org/10.2118/107416-MS

Raith, A., Wille, S., Horváth, B. & Zander-Schiebenhöfer, D., 2022. Integrity of the geological formation barrier-A comprehensive approach for the assessment of salt caverns. In *The Mechanical Behavior of Salt X* (pp. 545-552). CRC Press.

Realey, A., Elam, S., Grant, N., Ward, S. & Emsley, D. 2003. The Audrey Salt Wall and the Gas Field Beneath – Innovative Solutions to an Old Problem. European Association of Geoscientists & Engineers. Conference Proceedings, 65th EAGE Conference & Exhibition, Jun 2003, cp-6-00085. https://doi.org/10.3997/2214-4609-pdb.6.D07

Richter-Bernburg, G. 1980. Salt tectonics, Interior structures of salt bodies, Bulletin Centres Recherches Exploration-Production Elf-Aquitaine, 4(1):373-393.

Rowan, M.G., Urai, J.L., Carl Fiduk, J. & Kukla, P.A. 2019. Deformation of intrasalt competent layers in different modes of salt tectonics. Solid Earth, 10(3), 987–1013. https://doi.org/10.5194/se-10-987-2019.

Saltwork consultantsConsultants.com Pty Ltd. 2021. Solution mining. [online] available at: https://www.saltworkconsultants.com/solution-mining/ [Accessed 20 May 2021].

Scafidi, J., Wilkinson, M., Gilfillan, S., Heinemann, N., & Haszeldine, R. (2021). A quantitative assessment of the hydrogen storage capacity of the UK continental shelf. *International Journal of Hydrogen Energy, 46*(12), 8629-8639.

Schiro, F., Stoppato, A. & Benato, A. 2019. Potentialities of hydrogen enriched natural gas for residential heating decarbonization and impact analysis on premixed boilers, E3S Web of Conferences, proc. of International Conference on Advances in Energy Systems and Environmental Engineering (ASEE19), 116(00072), pp.8.

Schlumberger 1991. Log Interpretation Principles/Applications. Schlumberger Educational Services, Houston, 3rd printing. (Original printed in 1989).

Smith, D.B. 1979. Rapid marine transgressions and regressions of the upper Permian Zechstein Sea, J. Geol. Soc. 136:155–156, https://doi.org/10.1144/gsjgs.136.2. 0155.

Smith, N.J.P., Evans, D.J. & Andrew, I. 2005. The geology of gas storage in offshore salt caverns, Marine, Coastal and Hydrocarbons Programme, British Geological Survey, October, p.1-22.

Stolzenburg, K., Wietschel, M., Geneose, F., Michaelis, J., Lehmann, J., Miege, A., Krause, S., Donadei, S., Crotogino, F., Acht, A., & Horvath, P.-L. 2014. Integration von Wind-Wasserstoff-Systemen in das Energiesystem, Final report, 31 March, Berlin.

Stone, H.B.J., Veldhuis, I. & Richardson, R.N. 2009. Underground hydrogen storage in the UK Geological Society, London, Special Publications 2009, 313:217-226, https://doi.org/10.1144/SP313.13.

Strozyk, F., Urai, J.L., van Gent, H.W., de Keijzer, M. & Kukla, P.A. 2014. Regional variations in the structure of the Permian Zechstein 3 intrasalt stringer in the northern Netherlands: 3D seismic interpretation and implications for salt tectonic evolution. 2(4).

Taheri, S.R., Pak, A., Shad, S., Mehrgini, B., & Razifar, M. 2020. Investigation of rock salt layer creep and its effects on casing collapse. International Journal of Mining Science and Technology, 30(3):357–365, https://doi.org/10.1016/j.ijmst.2020.02.001.

Tarkowski, R. & Uliasz-Misiak, B. 2021. Use of underground space for the storage of selected gases ($CH_4$, $H_2$, and $CO_2$) – possible conflicts of interest. Gospod. Surowcami Miner. - Miner. Res. Manag. 37(1):141–160, https://doi.org/10.24425/gsm.2021.136290.

Taylor, J.C.M., 1998. Upper Permian - Zechstein. In: Glennie, K.W. (Ed.), Petroleum Geology of the North Sea: Basic Concepts and Recent Advances. Blackwell Science, Oxford, pp. 174–211.

Ter Heege, J.H., De Bresser, J.H.P. & Spiers, C.J. 2005a. Rheological behaviour of synthetic rocksalt: the interplay between water, dynamic recrystallisation and deformation mechanisms, J. Struct. Geol. 27(6):948-63.

Ter Heege, J.H., De Bresser, J.H.P. & Spiers, C.J. 2005b. Dynamic recrystallization of wet synthetic polycrystalline halite: dependence of grain size distribution on flow stress, temperature and strain. Tectonophysics 396(1–2):35-57.

Tractebel 2021. World's first offshore hydrogen storage concept developed by Tractebel and partners. https://tractebel-engie.com/en/news/2021/world-s-first-offshore-hydrogen-storage-concept-developed-by-tractebel-and-partners.

Tucker, M.E. 1991. Sequence stratigraphy of carbonate-evaporite basins: models and application to the Upper Permian (Zechstein) of northeast England and adjoining North Sea, J. Geol. Soc. 148:1019-1036, https://doi.org/10.1144/gsjgs.148.6.1019.

Uliasz-Misiak, B., Lewandowska-Śmierzchalska, J. & Matuła, R. 2021. Selection of underground hydrogen storage risk assessment techniques, Energies, 14(8049), https://doi.org/10.3390/en14238049.

Urai, J., Schmatz, J. & Kalver, J. 2019. Over-pressured salt solution mining caverns and leakage mechanisms. Report, Project KEM-17.

Urai, J.L., Schléder, Z., Spiers, C.J. & Kukla, P.A. 2008. Flow and transport properties of salt rocks, in R. Littke, U. Bayer, D. Gajewski & S. Nelskamp (eds), Dynamics of complex intracontinental basins: The Central European Basin System, Berlin, Springer, 277-290.

Valle-Falcones, L.M., Grima-Olmedo, C., Mazadiego-Martínez, L.F., Hurtado-Bezos, A., Eguilior-Díaz, S. & Rodríguez-Pons, R. 2022. Green Hydrogen Storage in an Underground Cavern: A Case Study in Salt Diapir of Spain. *Appl. Sci.* 2022, *12*, 6081. https://doi.org/10.3390/app12126081.

Van Gent, H., Urai, J.L., & de Keijzer, M. 2011. The internal geometry of salt structures - A first look using 3D seismic data from the Zechstein of the Netherlands. Journal of Structural Geology, 33(3):292-311, https://doi.org/10.1016/j.jsg.2010.07.005.

Von Berlepsch, T. 2017. 6 - Salt repository systems: Design development approach at the example of the Gorleben salt dome. In M. J. Apted & J. Ahn (Eds.), *Geological Repository Systems for Safe Disposal of Spent Nuclear Fuels and Radioactive Waste (Second Edition)* (Second Edi, pp. 145–162). Woodhead Publishing. https://doi.org/https://doi.org/10.1016/B978-0-08-100642-9.00006-2.

Wang, L., Bérest, P. & Brouard, B. 2015a. Mechanical Behavior of Salt Caverns: Closed-Form Solutions vs Numerical Computations. *Rock Mech Rock Eng* 48**,** 2369–2382. https://doi.org/10.1007/s00603-014-0699-1.

Wang, T., Yang, C., Ma, H., Daemen, J.J.K. & Wu, H. 2015b. Safety evaluation of gas storage caverns located close to a tectonic fault, Journal of Natural Gas Science and Engineering, 23: 281–293, https://doi.org/10.1016/j.jngse.2015.02.005.

Wang, J., Zhang, Q., Song, Z., & Zhang, Y. 2021. Experimental study on creep properties of salt rock under long-period cyclic loading. *International Journal of Fatigue, 143*, 106009.

Warren, J.K. 2006. Evaporites: Sediments, resources, hydrocarbons, p.1036, Berlin.

Warsitzka, M., Kley, J. & Kukowski, N. 2015. Analogue experiments of salt flow and pillow growth due to basement faulting and differential loading, Solid Earth, 6:9–31, https://doi.org/10.5194/se-6-9-2015.

Wassing, B., Groenenberg, R. & ter Heege, J. 2022. Modelling cyclic injection and withdrawal of gas for subsurface energy storage in salt caverns. In The Mechanical Behavior of Salt X (pp. 616-625). CRC Press.

Williams, J.D.O., Fellgett, M.W., Kingdon, A. & Williamson, J.P. 2015. In-situ stress orientations in the UK Southern North Sea: Regional trends, deviations and detachment of the post-Zechstein stress field. Marine and Petroleum Geology, 67:769-784, https://doi.org/10.1016/j.marpetgeo.2015.06.008.

Williams, J.D.O., Williamson, J.P., Parkes, D., Evans, D.J., Kirk, K.L., Sunny, N., Hough, E., Vosper, H. & Akhurst, M.C. 2022. Does the United Kingdom Have Sufficient Geological Storage Capacity to Support a Hydrogen Economy? Estimating the Salt Cavern Storage Potential of Bedded Halite Formations. *Journal of Energy Storage* 53 (2022): 105109.

Zheng, J., Zhang, X., Xu, P., Gu, C., Wu, B. & Hou, Y. 2016. Standardized equation for hydrogen gas compressibility factor for fuel consumption applications, International Journal of Hydrogen, 41:6610-6617.

Zijp, M.H.A.A., Huijgen, M.A., Wilpshaar, M., Bouroullec, R.J. & ter Heege, H. 2018. Stringers in salt as a drilling risk, Report no. TNO2018 R10975 by Nederlandse Organisatie voor Toegepast Natuurwetenschappelijk Onderzoek for Dutch State Supervision of Mines, pp.41.

**Figure Captions**

Figure 1. Northwest-southeast schematic cross-section (A-A') of Quadrant 47, SNS, of the lithostratigraphic internal geometry of the Zechstein Supergroup carbonate-evaporite depositional system (the approximate location of the cross section is shown in Fig. 10). The salt formations best suited for salt cavern engineering have been highlighted and formed the focus of this study. Modified after Taylor (1998); Duguid & Underhill (2010) and Grant *et al.,* (2019). *C*., Captanian; *G*., Guadalupian.

Figure 2. Schematic diagram of the possible internal geometries of a salt structure in the SNS, following the general rule of thumb of diapiric salt forming anticlinal structures. The general demands for geotechnical safety, cavern design and cavern depth range are highlighted.

Figure 3. The stepped methodological approach to derive the potential of developing offshore salt caverns for underground hydrogen storage divided into four key criterial subgroups. *CAPEX*, capital expenditures; *OPEX*, operating expenses; *KPI*, key performance indicator.

Figure 4. Examples of salt cavern gas storage facilities around the world, highlighting geometries, depth ranges, and relative volumes from existing storage sites. The loss of cavern volume in relation to cavern convergence over time is displayed from the Eminence salt cavern, which experienced a 40% volume loss (adapted from Warren, 2006). Volumes are taken from Clipsham *et al.,* 1965; Crotogino *et al.,* 2001; GeoStock, 2007; He *et al.,* 2017; Bérest *et al.,* 2019 and Barnett *et al.,* 2021).

Figure 5. Simplified schematic diagram highlighting the general demands for geotechnical safety and resulting derived design related uncertainties, in bedded salt structures. Cavern design; (a) bell-shaped, (b) capsule shape. The designs highlighted are also applicable to diapiric salt structures, however, they tend to be less vertically restricted resulting in the development of taller and smaller diameter cavern design.

Figure 6. Compressibility factor Z of hydrogen at different pressure-temperature conditions.

Figure 7: Density of hydrogen ($kg/m^3$) at different pressure-temperature conditions.

Figure 8. Summary stratigraphic column of the investigated reference wells penetrating the Audrey Salt Wall (located in Fig. 10). The depth range is capped to 2000 m in alignment with cavern design demands, greater depths are not suitable due to increased cavern closure rates and optimum cavern pressures. The locality optimising both depth, operational pressures and minimal insoluble inter-beds is suggested on each log. The locality of the cavern is subject to change once further ground investigation are conducted.

Figure 9. The methodological approach applied in this study in the derivation of the technical potential of offshore salt caverns for underground hydrogen storage, UKCS. Inset figures left to right: salt structure locality map adapted from Caglayan *et al.,* 2020; SNS bathymetry map and seismic section of the Audrey Salt Wall highlighting well 48/10-1 (5:1 vertical exaggeration).

Figure 10. Zechstein Supergroup isopach thickness map, produced by Maystrenko *et al*. (2012 and 2013) of the SNS, highlighting the areal limit of the study area. The primary type of salt domain can clearly be observed from the heterogeneity of salt thickness. It can be identified that low salt mobilisation regions are restricted to the western margin of the basin. In comparison towards the centre of the basin salt withdrawal basins adjacent to large diapiric structures dominate (examples displayed on map). The boreholes identified represent locations with salt volumes at suitable depth

ranges for salt cavern construction, based upon criteria established in Section *General cavern design demands* and Section *Weighted decision matrix ranking methodology*, and Tables 2 and 3. The number of locations presented was controlled by available offshore licence datasets during the completion this study (Table 4). The location of onshore operational, developing and dropped UK gas storage facilities on the east coastline are displayed (after Williams *et al.,* 2022). The inset in the top right corner displays the Zechstein Supergroup top depth map, SNS.

Figure 11. Seismic section (B – B') of the Audrey Salt Wall, SNS (Inline 28732). The location of the cross-section is highlighted in Figure 10 with the vertical axis displayed in two-way time (ms) (5:1 vertical exaggeration). The gamma ray log from well 48/10-1 is displayed. The highlighted area of seismic opaqueness as discussed in *Section 3.2* can be linked to borehole data from this region, which are interpreted to represent regions of halite (see Table 1 for gAPI properties of evaporates). Important seismic reflectors of geological time boundaries are highlighted on the RHS.

Figure A1: Forces acting on a gas volume of a cylindrical element with a cross section equal to $A$, when subject to hydrostatic equilibrium.

Supplementary Figure 1: Synthetic-seismic well tie of Well 41/05-1 (Inline 28732), displaying petrophysical log data. This well is located in a region of low salt mobilisation (highlighted in Figure 10), where the full stratigraphic sequence of the Zechstein Supergroup succession can be observed. Synthetic and seismic traces were calibrated to the timing of sonic and density logs, determined from the analysis of time-depth relationships from available well database checkshot surveys.

**Table Captions**

Table 1. Properties and petrophysical properties of selected evaporites, carbonates and mudstone (Schlumberger, 1991 and Urai *et al.,* 2008).

Table 2. Key parameters in cavern design to minimise geomechanical instability of the salt cavern

Table 3. Key geological and industrial indicators for salt cavern storage site suitability (adopted from Chadwick *et al.*, 2008)

Table 4. Summary information of the selected well locations (SNS UKCS) with salt configurations deemed suitable for salt cavern development and their suitability for gas storage, ranked in descending order from the well screening results. Depth values were primarily determined from the available borehole data.

Table 5. Geometrical data of the investigated caverns

Table 6. Summary of assumptions used in the cavern capacity calculations

Table 7. Results of the calculations for the hydrogen storage capacity of the two investigated caverns

| **Name** | **Composition** | **Solubility (at 20 °C) [g/l]** | **Density [kg/m$^3$]** | **Gamma-ray [API]** | **Sonic [ms/ft]** |
|---|---|---|---|---|---|
| Halite | NaCl | 264 | 2040 | 0 | 67 |
| Anhydrite | $CaCO_4$ | 1.97 | 2980 | 0 | 50 |
| Gypsum | $CaCO_4.2H_2O$ | 2 | 2350 | 0 | 52 |
| Sylvite | KCl | 340 | 1860 | 500 | 74 |
| Carnallite | $KMgCl_36H_2O$ or $MgCl_2.KCl.6H_2O$ | 273 | 1570 | 220 | 78 |
| Polyhalite | $K_2Ca_2Mg(SO_4)_4.2H_2O$ | 27 | 2790 | 180 | 57 |
| Dolomite | $CaMg(CO_3)_2$ | 0.055 | 2870 | 0 | 44 |
| Calcite | $CaCO_3$ | 0.052 | 2710 | 0 | 49 |
| Mudstone | - | - | 2200-2650 | 60-150 | 60-170 |



**Table 1**

| **Parameter** | **Value** | **Reference** |
|---|---|---|
| Cavern spacing (axis to axis) | 4 × cavern diameter | Caglayan *et al.* (2020) |
| Hanging-wall thickness | 75% of the cavern diameter | Caglayan *et al.* (2020) |
| Footwall thickness | 20% of the cavern diameter | Wang *et al.* (2015b) |
| Cavern height:diameter ratio | >0.5 | Wang *et al.* (2015b) |
| Cavern shape | bell-shaped / cylindrical-shaped | Lux (2009) |
| Cavern depth range | 500 m – 2,000 m | Plaat (2009); Evans & Holloway (2009) and Caglayan *et al.* (2020) |
| Distance from adjacent faults/discontinuities or subsurface man-made features (e.g., abandoned hydrocarbon wells) | >2 × cavern diameter | Wang *et al.* (2015b) |
| Operating $H_2$ pressure (measured at the last cemented casing shoe) | $p_{min}$ = 24%, $p_{max}$ = 80% of geostatic vertical stress. | Ozarslan (2012) and Stolzenburg *et al.* (2014) |
| Distance from salt formation edge | >500 m (diapiric)<br>>2,000 m (bedded) | Kupfer *et al.* (1998) and Caglayan *et al.* (2020) |



**Table 2**

| Parameter | Criteria | Positive indicator score = 10 | Intermediate indicator score = 5 | Cautionary indicator score = 1 | Reference |
|---|---|---|---|---|---|
| Host salt formation | Depth [m] (from seabed) | 1,000-1,500 | 500-1,000 & 1,500-2,000 | < 500 & > 2,000 | Smith *et al.*, 2005; Plaat, 2009; Evans & Holloway, 2009 and Caglayan *et al.*, 2020 |
| | Thickness [m] | > 400 | 200-400 | < 200 | Caglayan *et al.*, 2020 and Own data |
| | Purity [%] | > 80 | 60-80 | < 60 | Li *et al.*, 2019; Saltwork Consultants, 2021 |
| | *In situ* stress state | Isotropic | Orthotropic | Anisotropic | Minkley *et al.*, 2015; Li & Urai, 2016; Zijp *et al.*, 2018 and Urai *et al.*, 2019 |
| Load bearing rock formation (hanging- and foot-wall) | Lithology | Halite | Mudstone & K/Mg salts | Carbonate & Anhydrite | Li *et al.*, 2020 and Taheri *et al.*, 2020 |
| | Thickness [m] | Bedded hanging: > 80; foot: > 30 Diapiric hanging: > 50; foot: >15 | Bedded hanging: 63; foot: 16.8 Diapiric hanging: > 43.5; foot: 11.6 | Bedded hanging: < 60; foot: < 20 Diapiric hanging: < 40; foot: < 10 | Bruno, 2005; Wang *et al.*, 2015b and Caglayan *et al.*, 2020 |
| | Structural features | None | Folding | Faults/fractures | Own data |
| Lithological Interlayers | Lithology | K/Mg Salts & Polyhalite | Anhydrite & Mudstone | Carbonates | Li & Urai, 2016; Cala *et al.*, 2018; Zijp *et al.*, 2018 and Urai *et al.*, 2019 |
| *If no interlayers award score = 100* | Thickness [m] (non-salt) | < 3 (single interlayer) | 3 (single interlayer) | > 3 (single interlayer) | Hamilton, 1971 |
| | Thickness [m] (K-Mg salts) | < 3 (total thickness) | 3-10 (total thickness) | > 10 (total thickness) | Urai *et al.*, 2019 |
| | Location | Base | Centre | Top | Richter-Bernburg, 1980; Crotogino, 2016 and Li *et al.*, 2019 |
| | Number of interlayers | 0 | 1-2 | > 2 | Li & Urai, 2016; Cala *et al.*, 2018; Zijp *et al.*, 2018 and Urai *et al.*, 2019 |
| Cavern geometry | Cavern volume [$m^3$] (cavern height [m]) | 750,000 (300) | 500,000 (120) | N/A | Caglayan *et al.*, 2020 |
| | Distance from salt edge [m] | Bedded: 2,000 Diapiric: 1,000 | Bedded: < 2,000, > 500 Diapiric: < 1,000, > 500 | < 500 m | Kupfer *et al.*, 1998; Looff *et al.*, 2003 and Caglayan *et al.*, 2020 |
| Industrial | Pipeline infrastructure [km] | < 5 | 5 - 10 | > 10 | Own data |
| | Distance from UK coastline [km] | < 50 | 50 - 80 | > 80 | Own data |

**Table 3**

| Reference Well | Formation | Salt Bed/package Thickness [m] | Top Depth of Cavern Placement (from seabed) [m] | Halokinesis / Salt Domain | Purity / Heterogeneity | Comments and suitability for gas storage |
|---|---|---|---|---|---|---|
| *48/10-1* | *Z2 & Z3 salts* | *>775* | *~1145* | *Salt Wall* | *Thick halite, with minimal insoluble* | *High potential* |
| *43/28a-3* | *Undifferentiated Z2 to Z4 salts* | *>750* | *~1080* | *Salt Diapir* | *Halite* | *High potential* |
| *42/28b-7* | *Z3 & Z4* | *>470* | *~965* | *Salt Diapir* | *Halite* | *High potential* |
| *42/29-5* | *Z3* | *>640* | *~1115* | *Salt Diapir* | *Thick halite* | *High potential* |
| *44/29-3* | *Undifferentiated Z2 to Z4 salts* | *>500* | *~1510* | *Salt Diapir* | *Thick halite* | *High potential* |
| *49/01-1* | *Undifferentiated Z2 to Z4 salts* | *>1165* | *~700* | *Salt Wall* | *Thick halite* | *High potential* |
| *49/07b-2* | *Undifferentiated salts* | *>410* | *~1530* | *Salt Wall* | *Halite* | *High potential* |
| *42/28b-5* | *Z4* | *>330* | *~1175* | *Salt Diapir* | *Halite* | *Good potential but vertically restricted.* |
| *41/05-1* | *Z2* | *>350* | *~1500* | *Bedded salt* | *Halite* | *Good potential but vertically restricted by non-salt lithologies.* |
| *47/05-1* | *Z4* | *>240* | *~1705* | *Salt Wall* | *Halite* | *Good potential but vertically restricted by non-salt lithologies and cavern depth limit.* |
| *48/15a-3* | *Undifferentiated Z2 to Z4 salts* | *>1190* | *~980* | *Salt Wall* | *Thick halite* | *High potential* |
| *48/03-4* | *Undifferentiated Z3 to Z4 salts* | *>300* | *~1730* | *Salt Wall* | *Halite* | *Good potential but vertically* |

| | | | | | | |
|---|---|---|---|---|---|---|
| | | | | | | *restricted by non-salt lithologies and cavern depth limit.* |
| *47/10-4* | *Undifferentiated Z2 to Z4 salts* | *>420* | *~1550* | *Salt Diapir* | *Thick halite, interbedded with high % of K-Mg salts* | *High potential* |
| *49/16-12* | *Undifferentiated Z2 to Z4 salts* | *>1250* | *~840* | *Salt Diapir* | *Thick halite* | *High potential* |
| *49/02-3* | *Undifferentiated Z3 to Z4 salts* | *>850* | *~1670* | *Salt Diapir* | *Thick halite, with minimal insoluble* | *Good potential but vertically restricted due to cavern depth limit.* |
| *48/10a-14* | *Undifferentiated Z2 to Z4 salts* | *>780* | *~1070* | *Salt Wall* | *Thick halite, with a high % of K-Mg salts* | *Good potential but may have higher creep rate due to high % of K-Mg salts.* |
| *41/10-1* | *Z2* | *>310* | *~1670* | *Bedded salt* | *Halite* | *Good potential but vertically restricted by non-salt lithologies.* |



**Table 4**

| Parameter | Cavern A | Cavern B |
|---|---|---|
| Cavern total volume [$m^3$] | 500,000 | 750,000 |
| Cavern free volume [$m^3$] | 350,000 | 525,000 |
| Depth to cavern roof from seabed [m] | 1,200 | 1,620 |
| Maximum cavern diameter [m] | 84 | 58 |
| Cavern height [m] | 120 | 300 |



**Table 5**

| **Parameter** | **Value** |
|---|---|
| Seabed depth | 50 m |
| Fraction of total cavern volume used as cavern free volume | 70% |
| Average temperature at wellhead | 6°C |
| Height of cavern neck | 40 m |
| Maximum cavern pressure, specified at the LCCS | $0.80 \times \sigma_v$ |
| Minimum cavern pressure, specified at the LCCS | $0.24 \times \sigma_v$ |
| Average temperature at seabed | 9°C |
| Geothermal gradient | 0.031°C/m |



**Table 6**

| Calculations results | Cavern A | Cavern B |
|---|---|---|
| Depth of the LCCS, measured from the seabed level [m] | 1,160 | 1,580 |
| Geostatic vertical stress at the LCCS depth [bar] | 266.0 | 360.5 |
| Maximum cavern pressure, specified at the LCCS [bar] | 213.0 | 288.0 |
| Minimum cavern pressure, specified at the LCCS [bar] | 64.0 | 87.0 |
| Temperature at the LCCS depth [°C] | 45.0 | 58.0 |
| Temperature at cavern mid-height [°C] | 47.7 | 62.8 |
| Cushion hydrogen required to maintain minimum cavern pressure [$Sm^3$] | 19,885,600 | 38,733,000 |
| Net energy stored in the cavern [$MWh_{H2}$] | 119,500 | 219,100 |
| Energy density per cavern [$MWh_{H2}/Sm^3$] | 0.341 | 0.417 |



**Table 7**

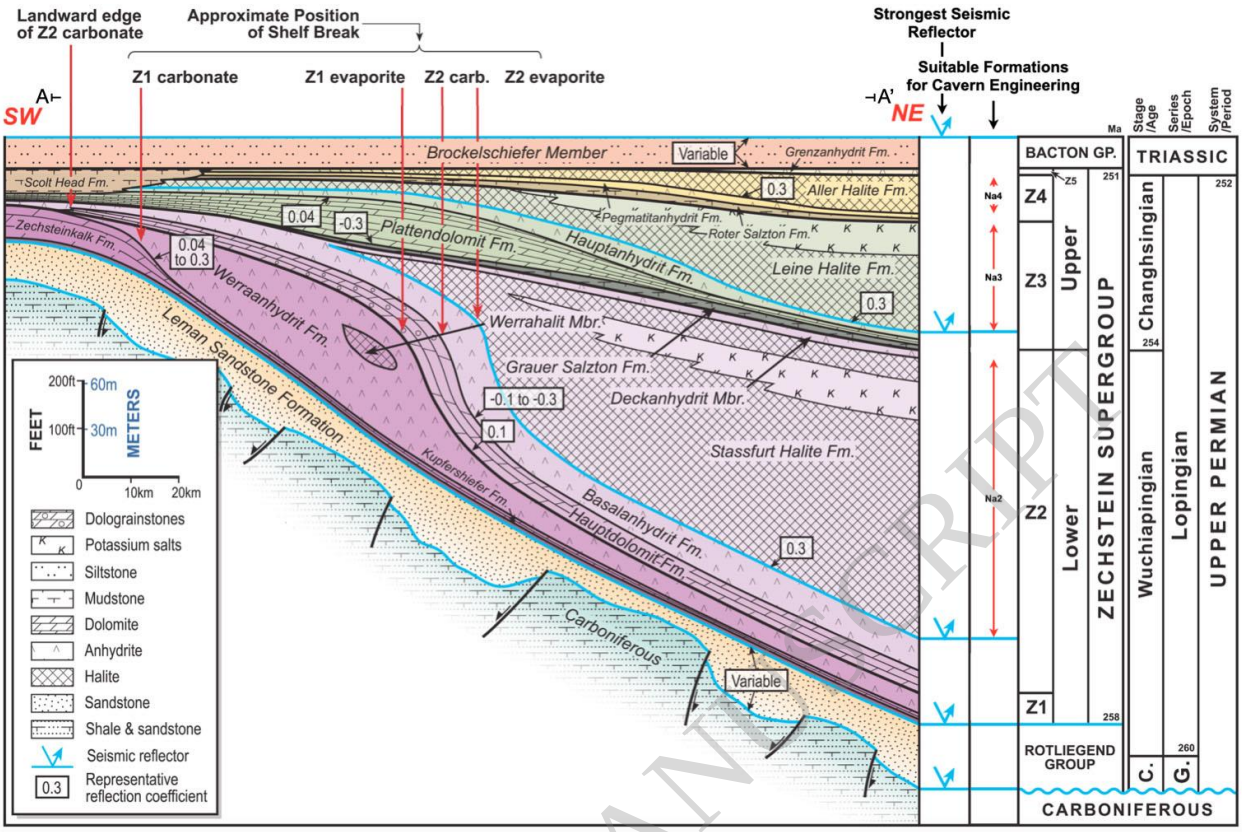




**Figure 1**

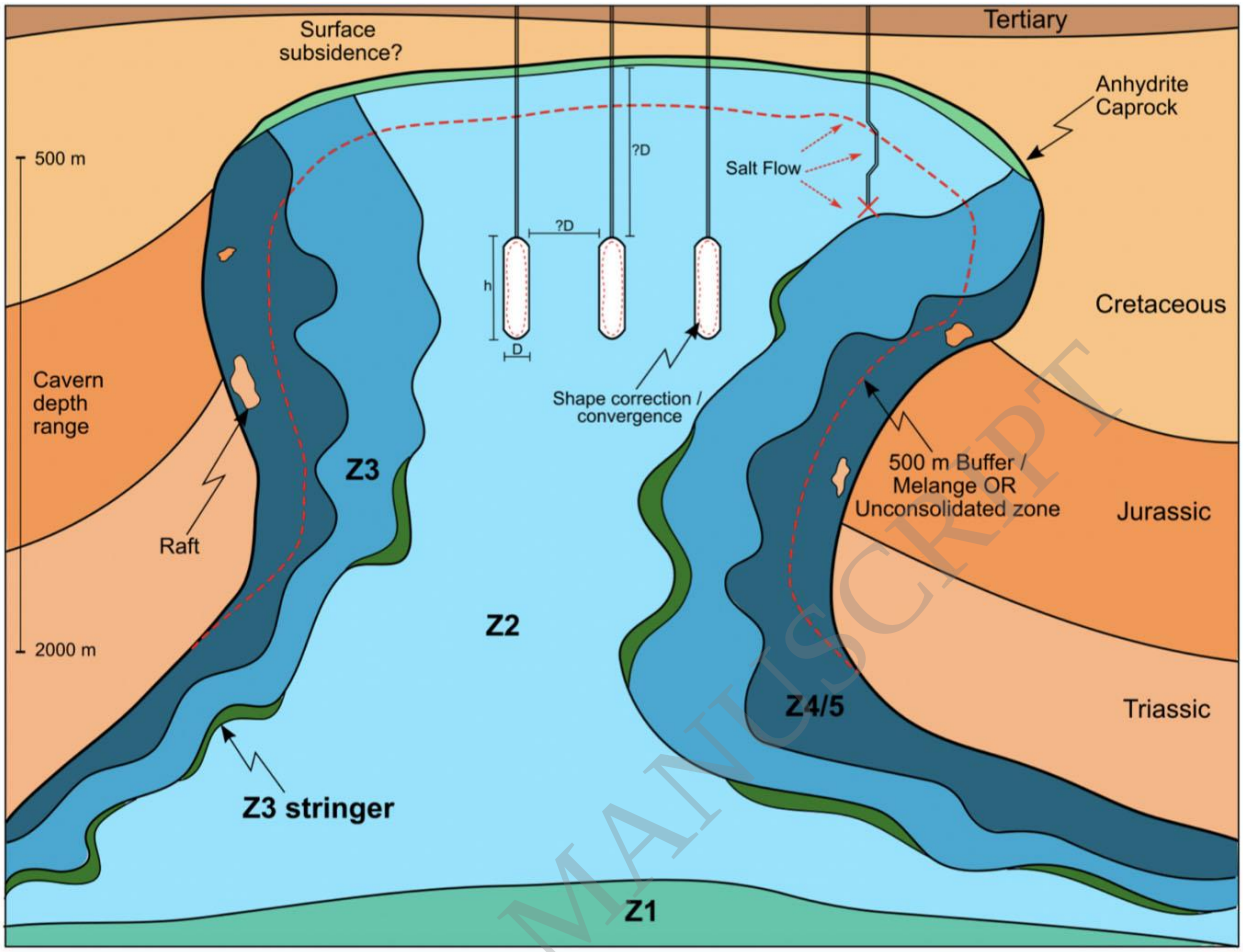




**Figure 2**

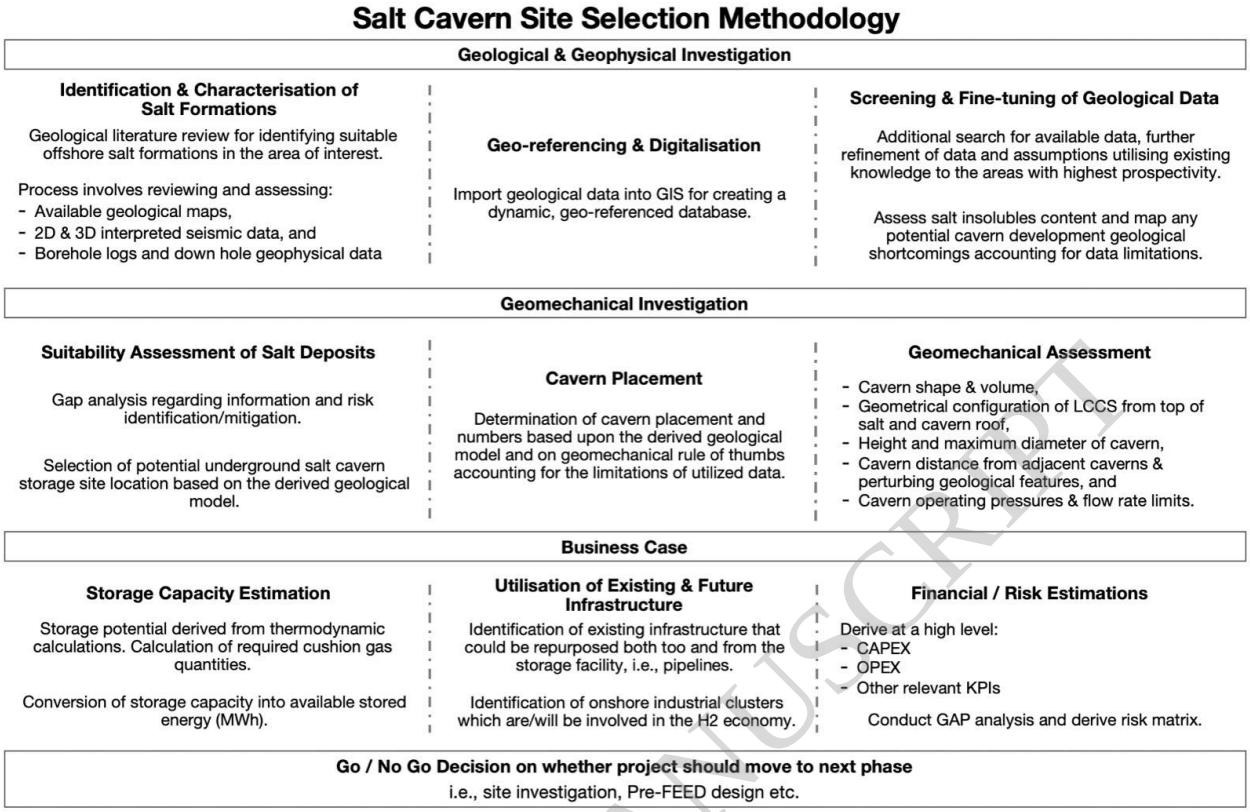




**Figure 3**

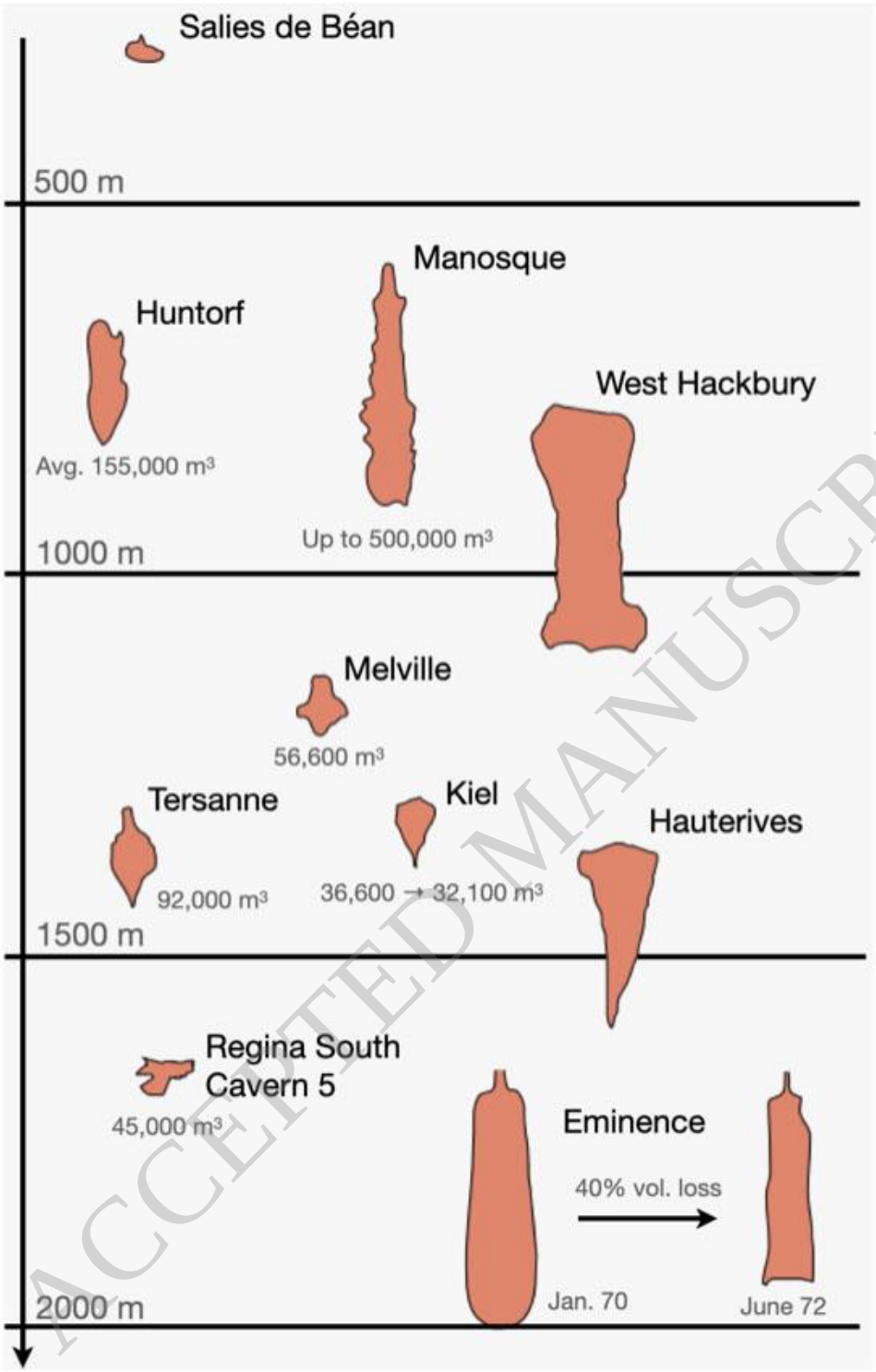




**Figure 4**

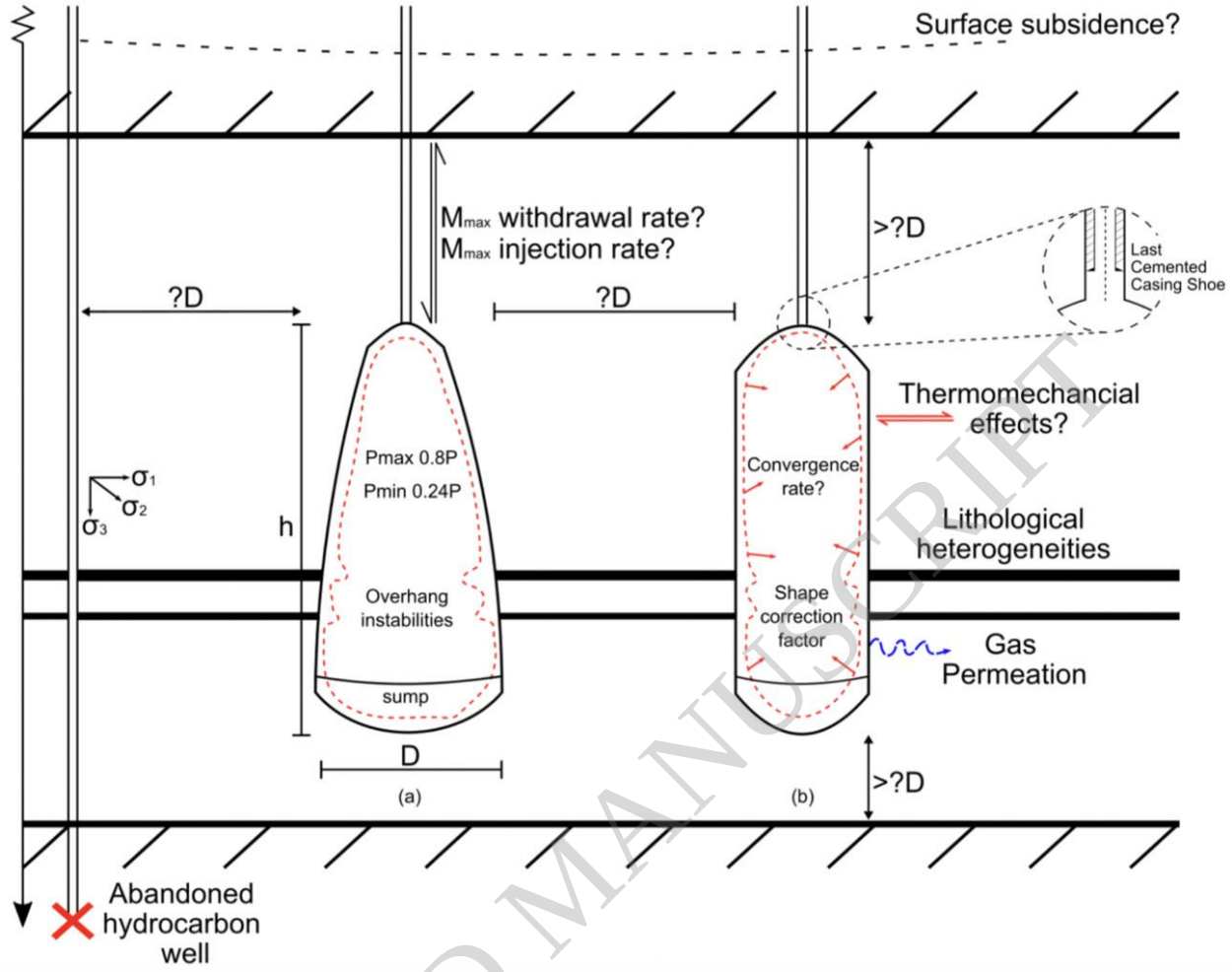




**Figure 5**

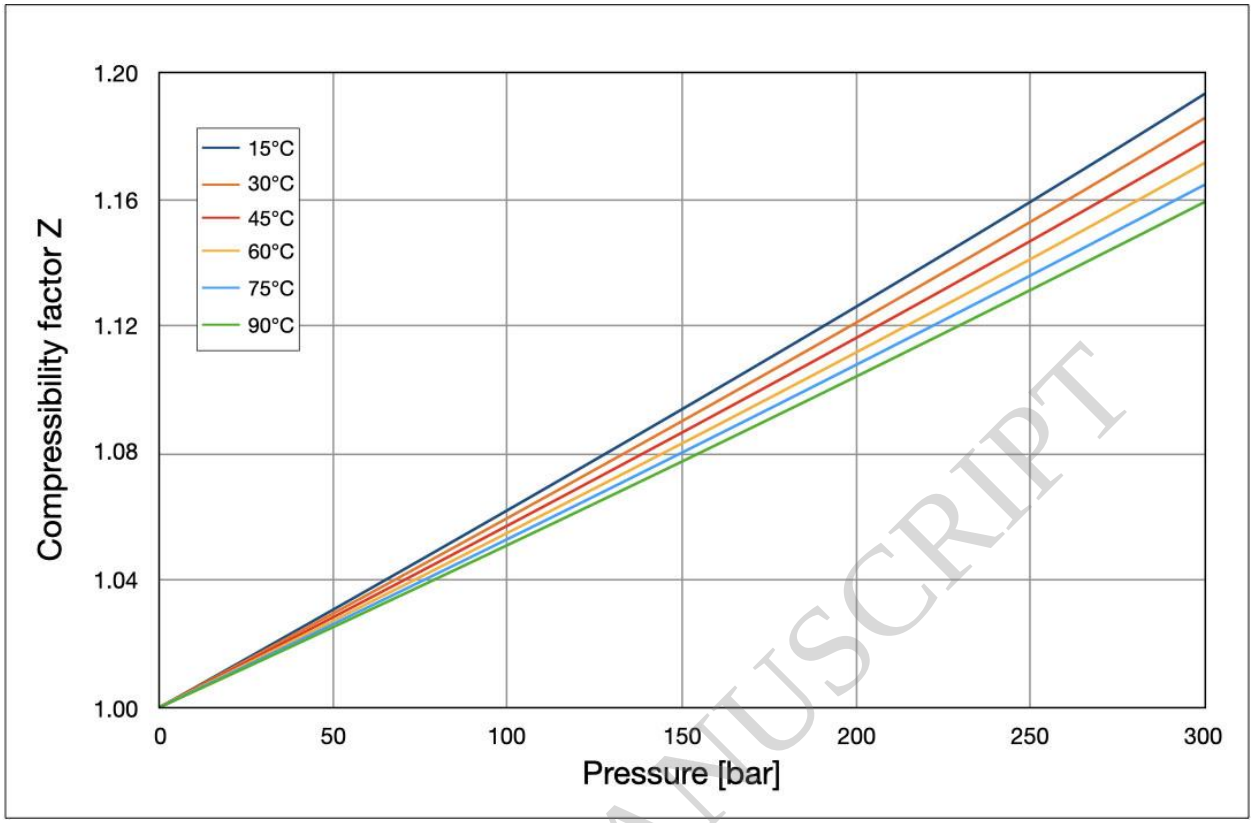




**Figure 6**

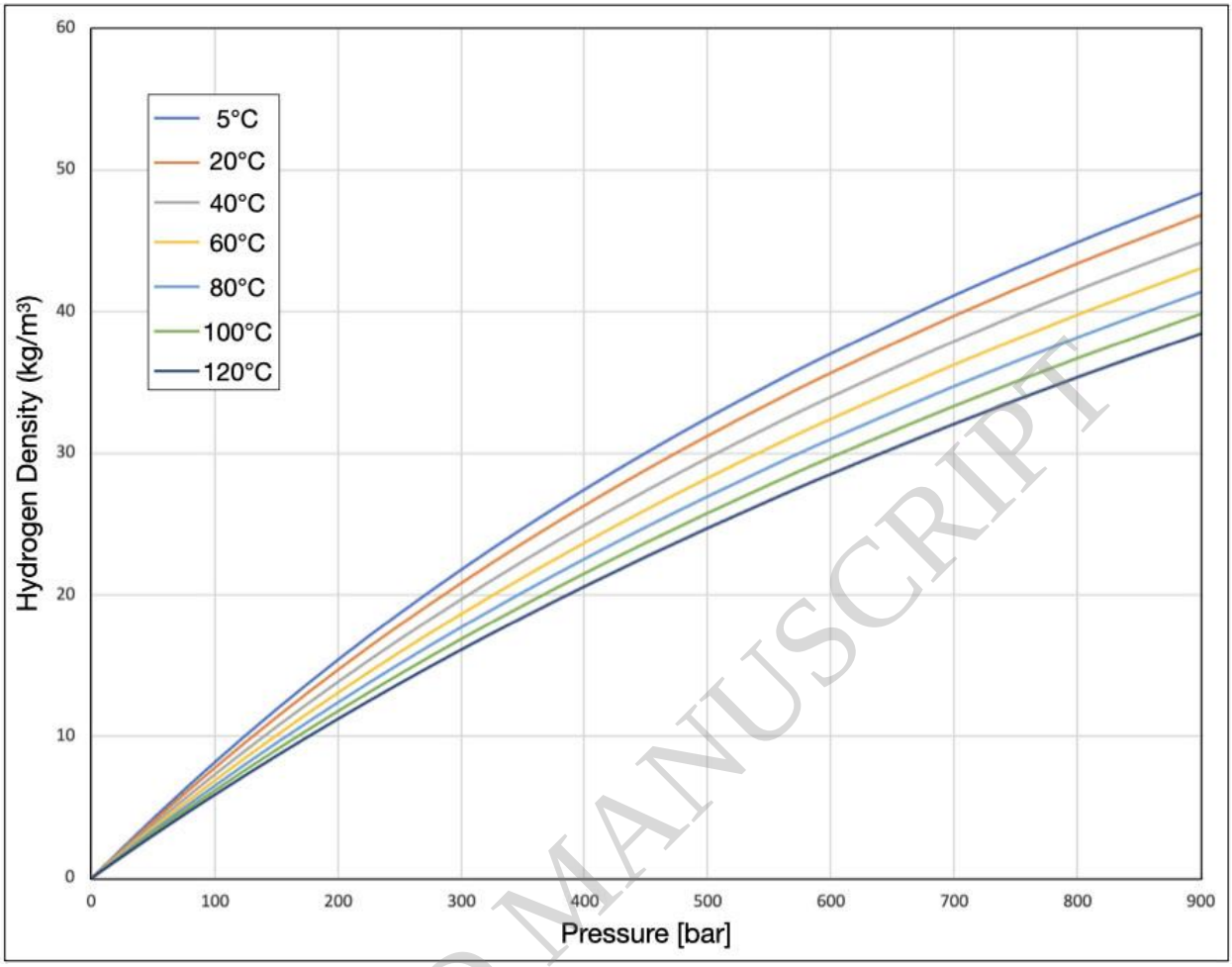




**Figure 7**

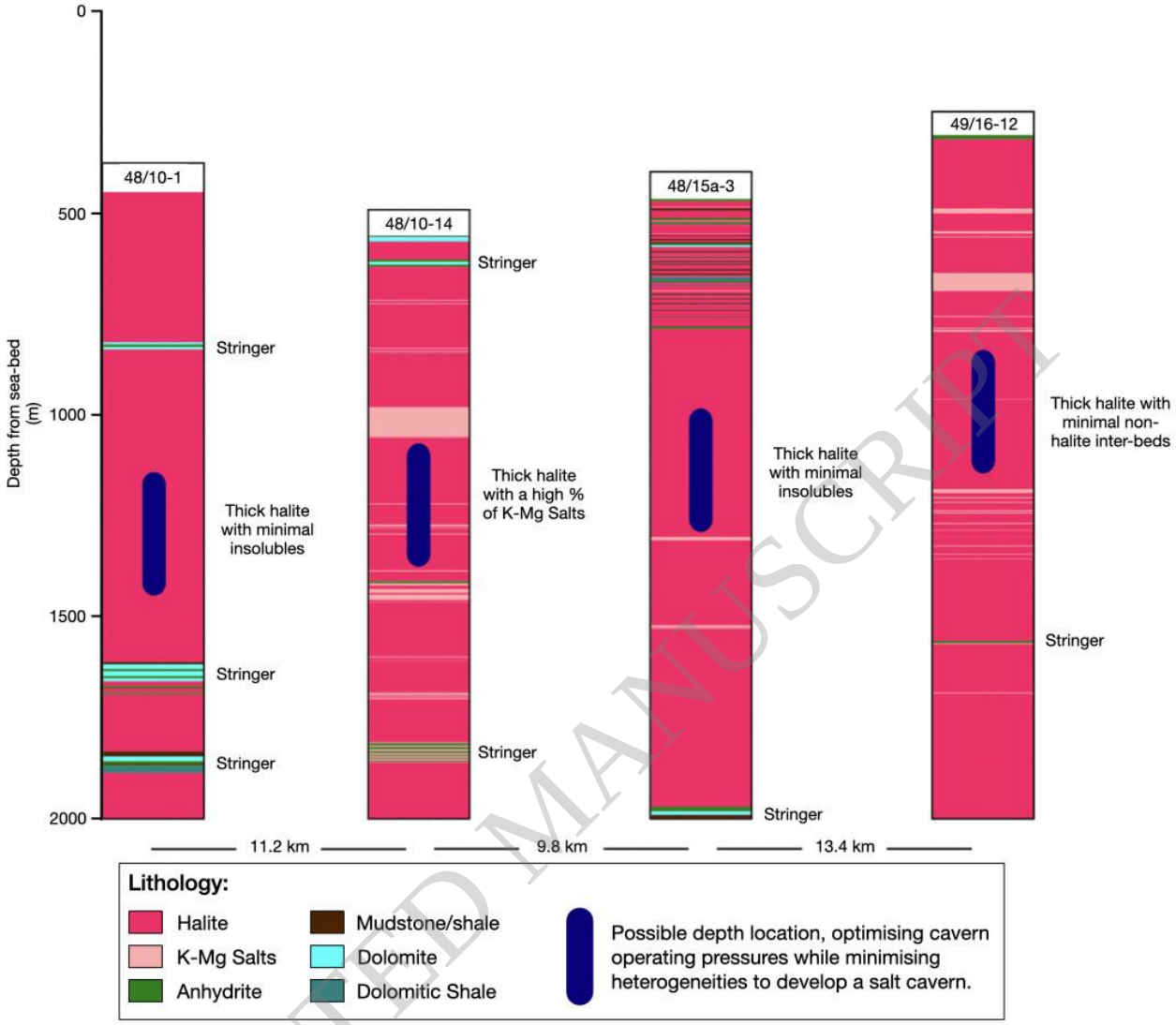




**Figure 8**

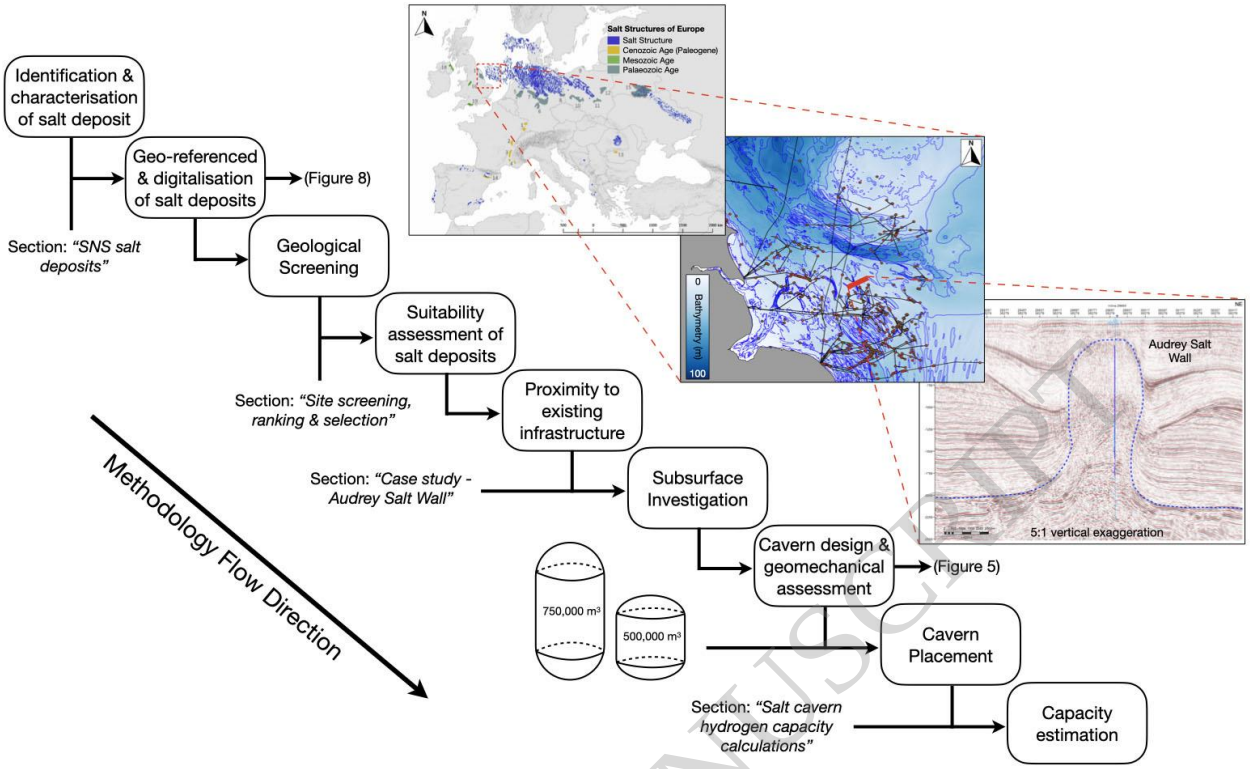




**Figure 9**

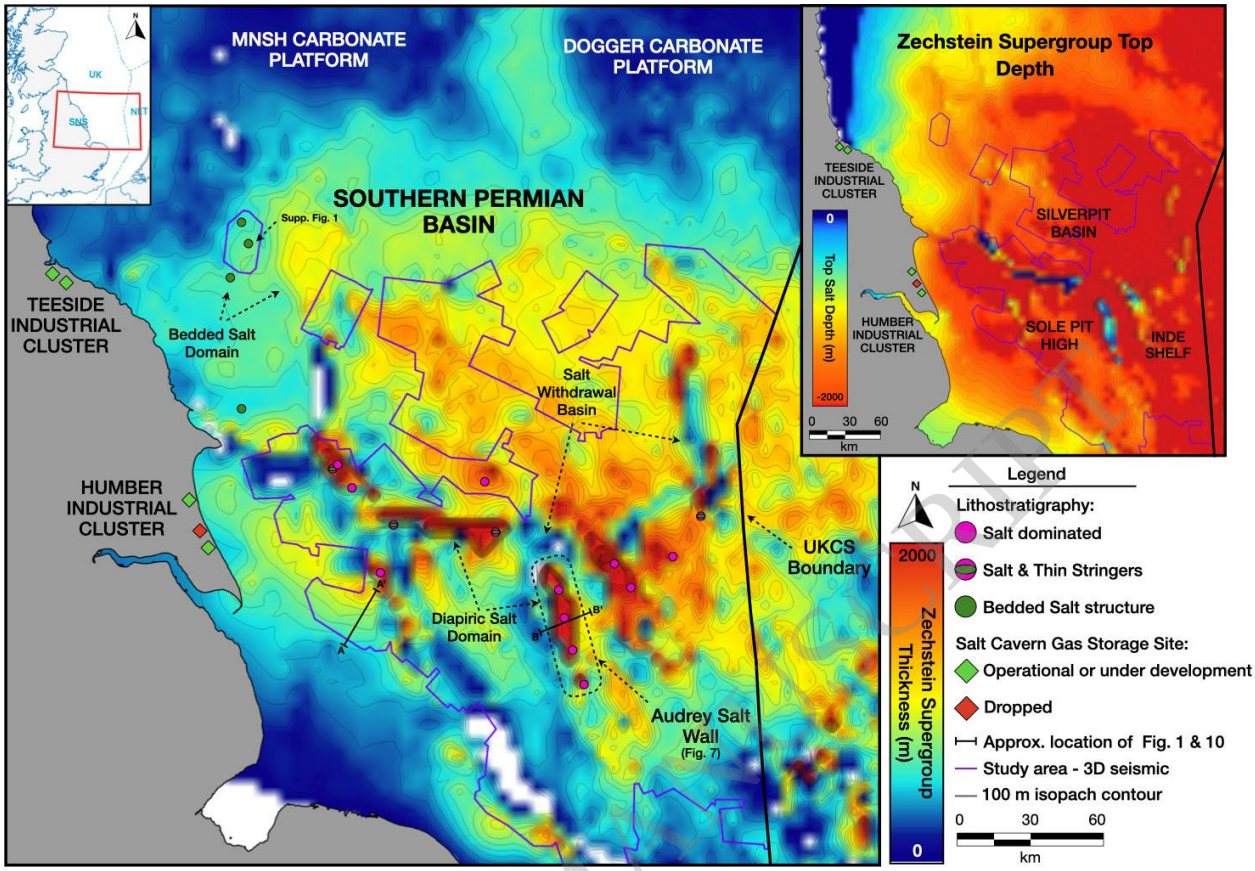




**Figure 10**

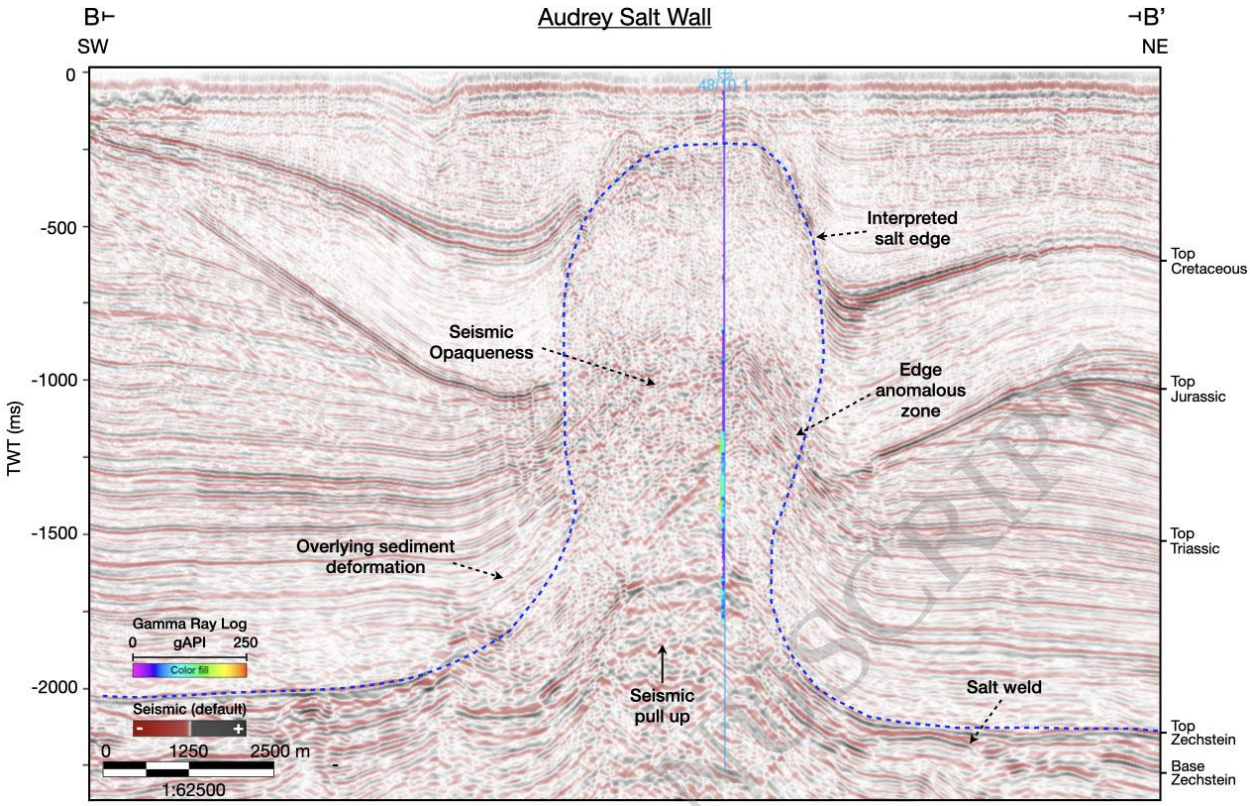




**Figure 11**

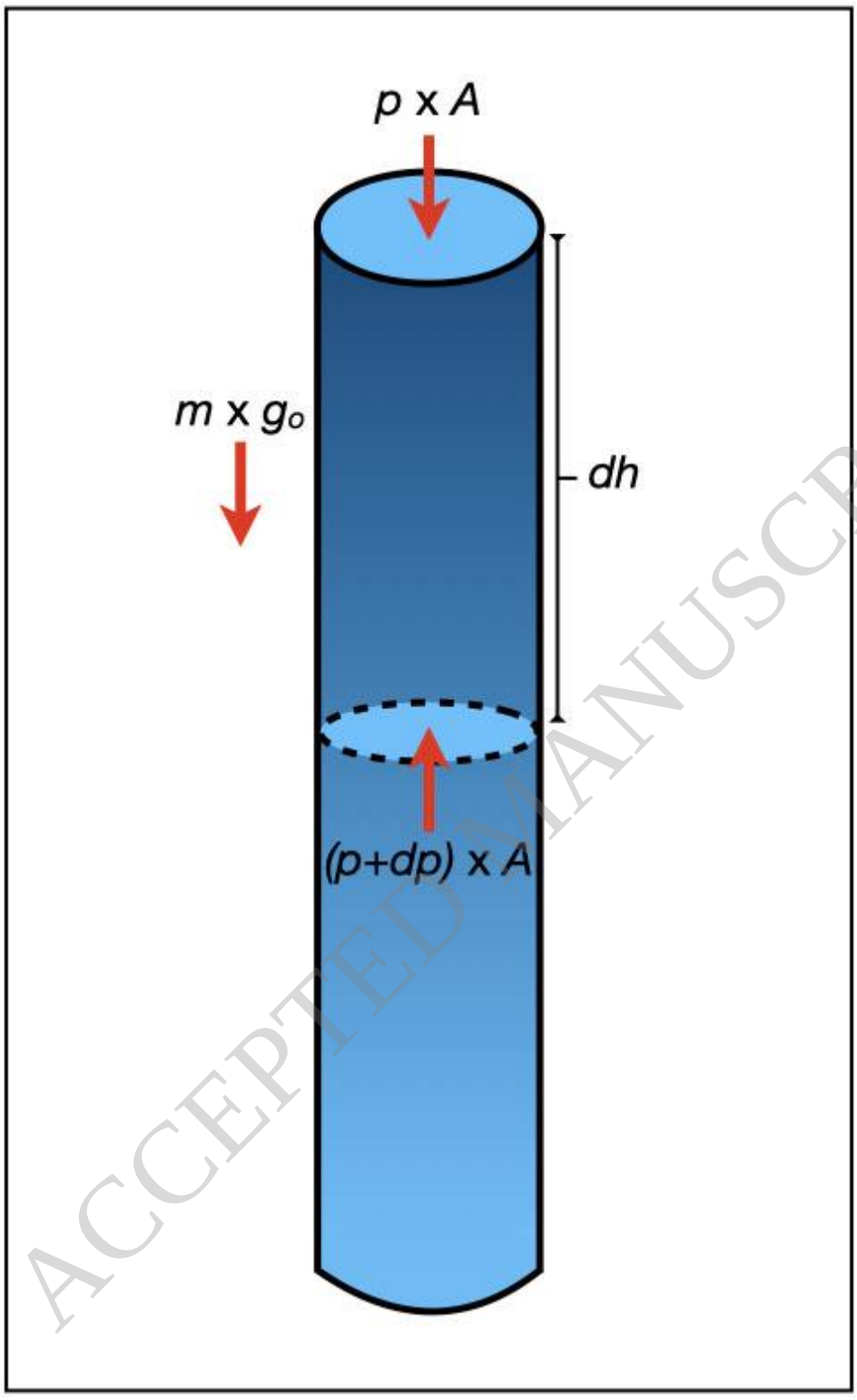


**Figure A1**